NATURAL RUBBER/ REDUCED GRAPHENE OXIDE (rGO) COMPOSITE DEVELOPMENT

PUA SHAH WEI

A project report submitted in partial fulfilment of the
requirements for the award of the degree of
Bachelor of Engineering (Hons) Petrochemical Engineering

Faculty of Engineering and Green Technology
Universiti Tunku Abdul Rahman

January 2016

DECLARATION

I hereby declare that this project report is based on my original work except for citations and quotations which have been duly acknowledged. I also declare that it has not been previously and concurrently submitted for any other degree or award at UTAR or other institutions.

Signature : _____

Name : Pua Shah Wei

ID No. : 11AGB05708

Date : _____

APPROVAL FOR SUBMISSION

I certify that this project report entitled "NATURAL RUBBER/ REDUCED GRAPHENE OXIDE (rGO) COMPOSITE DEVELOPMENT" was prepared by PUA SHAH WEI has met the required standard for submission in partial fulfilment of the requirements for the award of Bachelor of Engineering (Hons) Petrochemical Engineering at Universiti Tunku Abdul Rahman.

Approved by,

Signature : _____

Supervisor : Dr. Yamuna A/P Munusamy

Date : _____

Specially dedicated to

My beloved parents, Pua Ching Jo and Eng Bee Eng

ACKNOWLEDGEMENTS

I would like to thank everyone who had contributed to the successful completion of this project. I would like to express my gratitude to my research supervisor, Dr. Yamuna Munusamy for her invaluable advice, guidance and her enormous patience throughout the development of the research. My sincere thanks also goes to Dr. Mathialagan Muniyadi for all the support and advices.

Besides, I would like to acknowledge the support provided by Platinum Senawang Sdn. Bhd. and Universiti Sains Malaysia. In addition, I would also like to express my gratitude to my loving parent and friends who had helped and given me encouragement during the research.

NATURAL RUBBER/ REDUCED GRAPHENE OXIDE (rGO) COMPOSITE DEVELOPMENT

ABSTRACT

In recent years, graphene-based nanofillers have gathered attention worldwide academically and in industry. It has been proposed as a promising new material due to its outstanding physical properties such as high electron mobility, thermal conductivity, mechanical stiffness, strength and elasticity. In this research, natural rubber (NR)/ reduced graphene oxide (rGO) nanocomposites was prepared at different loading using two roll mill. Morphology study of the nanocomposites showed that at 1.0 phr rGO loading, the best dispersion of the filler in rubber matrix was achieved. Agglomeration occured in NR/1.5 phr rGO nanocomposites as shown by field emission scanning electron images (FESEM). The optimum properties was obtained at 1.0 phr rGO loading with tensile strength of 18.46 MPa, modulus at 100% elongation of 6.63 MPa, modulus at 300% elongation of 7.73 MPa. However, NR/ 1.0 phr rGO composite showed the lowest elongation at break of 501.60%. The highest hardness value of 46.7 HRA was also achieved for NR/ 1.0 phr rGO. Chemical resistance study revealed that NR/ 1.0 phr rGO nanocomposite exhibit the highest chemical resistance with Mol % uptake of 1.24 and 1.03 for toluene and n-hexane respectively. The Swelling Index were 1.15 and 0.88 for toluene and n-hexane respectively.

TABLE OF CONTENTS

LIST OF TABLES

LIST OF FIGURES

LIST OF SYMBOLS/ ABBREVIATIONS

℃	degree celcius
mm	millimetre
min	minute
rpm	revolution per minute
g	gram
ml	millilitre
MPa	mega pascal
HRA	rockwell hardness unit
%	percentage
S	siemens
cm	centimetre
V	volt
nm	nanometer
phr	parts per hundred rubber
dNm	deci newtown meter
μm	micrometer
GPa	giga pascal
TPa	tera pascal
W	watt
mK	milli kelvin
kc	kilocycles

GO	graphene oxide
rGO	reduced graphene oxide
AFM	atomic force microscopy
CNTs	carbon nanotubes
Cu	copper
$KMnO_4$	potassium permanganate
H_2SO_4	sulphuric acid
$KClO_3$	potassium chlorate
$NaClO_3$	sodium chlorate
HNO_3	nitric acid
CVD	chemical vapour deposition
TEGO	thermally expanded graphite oxide
CO	carbon monoxide
CO_2	carbon dioxide
NO_2	nitrogen dioxide
N_2O_4	dinitrogen tetroxide
Mn_2O_7	manganese heptoxide
$K_2S_2O_8$	potassium persulfate
P_2O_5	phosphorus pentoxide
$NaNO_3$	sodium nitrate
H_3PO_4	phosphoric acid
XPS	x-ray photoelectron spectroscopy
MWI	microwave irradiation
$NaBH_4$	sodium borohydride

VC	vitamin c
KNO_3	potassium nitrate
NR	natural rubber
ENR	epoxidized natural rubber
OPA	oil palm ash
LENR	liquid epoxidized natural rubber
TGA	thermogravimetric analysis
PPy	polypyrrole
PA	palygorskite
CeO_2	cerium oxide
CTAB	cetyl-trimethylammonium bromide
MMT	montmorillonite
EOMt	expanded organo-montmorillonite
PANI	polyaniline
EMI	electromagnetic interference
PVA	polyvinyl alcohol
PS	polystyrene
PMMA	polymethylmethacrylate
EG	expanded graphite
GNPs	graphene nanoplatelets
THF	tetrahydrofuran
DMF	dimethyl formamide
PE-g-MA	polyethylene-grafted maleic anhydride
PP	polypropylene

HDPE	high dense polyethylene
PPS	polyphenylene sulphide
PA6	polyamide
GNF	graphite nanofiber
DI	deionized
HCl	hydrochloric acid
H_2O_2	hydrogen peroxide
SMR10	standard Malaysia rubber grade 10
ZnO	zinc oxide
t_{90}	cure time
t_{S2}	scorch time
ML	minimum torque
MH	maximum torque
CRI	cure rate index
FTIR	fourier transform infrared spectrophotometer
XRD	x-ray diffraction
FESEM	field emission scanning electron microscope
J.I.S	japanese industrial standard
SI	swelling index
NR/ rGO	reduced graphene oxide filled natural rubber nanocomposites

LIST OF EQUATIONS

LIST OF APPENDICES

CHAPTER 1

INTRODUCTION

1.1 Background

Rubbers have been mixed with reinforcing fillers to enhance their mechanical properties, thermal stability and oil resistance. Rubbers without filler would have very restricted applications due to their poor mechanical and physical properties. One of the industries that requires huge amount of filled rubber is the tire industry. The most widely used filler for rubber in tire industry is carbon black. A huge number of previous research studies have reported small amounts of particulate fillers such as carbon-black can introduce remarkable changes in the mechanical and physical properties of rubber (Li et al., 2012).

The extent of property improvement depends on several parameters including the size of the particles, their aspect ratio, their degree of dispersion and orientation in the matrix and the degree of adhesion with the rubber chains (Bokobza. L, 2004). At present, nanofillers have attracted much attention from rubber scientists because of their small size and the corresponding increase in the surface area for interaction with rubber chains. This lead to achievement of required mechanical properties at low filler loadings. (Arroyo et al., 2003). The incorporation of nanofillers such as graphene, graphite oxide and reduced graphite oxide into polymer matrix creates materials that show improved physical, mechanical, dynamic mechanical, thermal, and other properties.

Recently, graphene has become well-known as a reinforcing material due to its outstanding characteristics such as high electron mobility, mechanical stiffness, thermal conductivity (K), strength and elasticity. Graphene is a single layer form of graphite packed in hexagonal shape. Although graphene had been studied theoretically for decades, its actual existence was not proven until 2004, when Kostya Novoselov and Andrei Geim from the Manchester University managed to isolate a monolayer of graphene from graphite for the first time. In 2010 they were awarded the Nobel Prize (Choi and Lee, 2012). Figure 1.1 shows the structure of carbon atom arrangement in graphene.

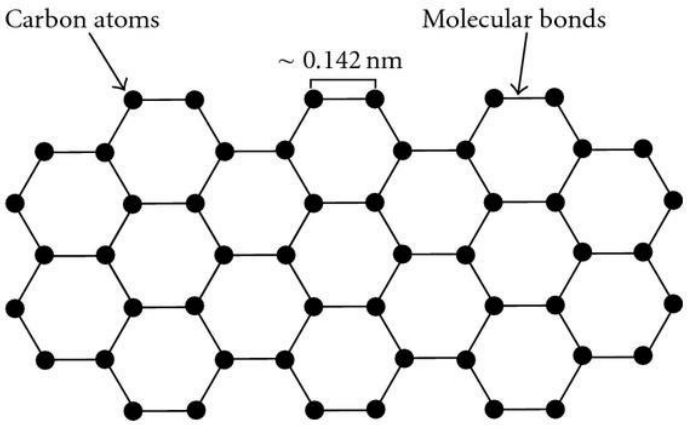

Figure 1.1: Structure of carbon atom arrangement in graphene (Roberts et al., 2010)

Graphene oxide (GO) can be produced through either Hummers or Brodie method as these two methods both are for the oxidation of graphite where carboxyl, hydroxyl and epoxide functional groups are introduced at the basal planes and edges of graphite. Chemical reduction of GO is the most widely applied technique for preparing chemically reduced graphene oxide (rGO) nanosheets, which is one of the most popular chemically converted graphene (Xinmeng et al., 2014). Either rGO or GO could be selected as reinforcing fillers for polymers based on the polymer chemical functionalities. GO are normally selected as filler for polymers with hydrophilic functionalities and rGO is commonly selected for hydrophobic polymers.

1.2 Problem Statement

Graphene is chemically inert; this prevents it from having interaction with rubber when they were mixed together. Besides, low solubility of graphene limits its applications. As nanofiller, the amount added into the rubber will be very little. Graphene needs to be well dispersed and homogenized when added into the rubber. In order to overcome these problems, derivatives of graphene, GO and rGO were used. In term of strength, both GO and rGO have similar strength. However, it is expected that hydrophilic GO will not disperse well in hydrophobic natural rubber matrix. Therefore, we intend to reduce the GO to rGO as rGo is less hydrophilic compared to GO.

In this study, rGO were incorporated in natural rubber. The optimum loading in the range of 0 phr to 1.5 phr was determined. Low loading range is preferred because the price of graphene is very expensive. Besides, the performance of the pure natural rubber and nanocomposites were also tested and compared in terms of hardness, tensile strength, fatigue and swelling. The morphology of the nanocomposites was also examined.

1.3 Objectives

The objectives of this study are:

- To produce natural rubber/ reduced graphene oxide (rGO) composite with different loading of rGO.
- To test the curing, mechanical, thermal and physical properties of the rubber nanocomposites.

CHAPTER 2

LITERATURE REVIEW

2.1 Overview of Graphene

Graphene was first discovered by Novoselov and Geim via mechanical exfoliation of graphite using scope tape in year 2004. It is also known as the first discovered two-dimensional (2D) crystalline material in the world (Geim and Novoselov, 2007). Graphene is a single layer of carbon packed in a hexagonal honeycomb lattice, with a carbon-carbon distance of 0.142 nm. The dimension is monoatomic (≈3.3 Å) in one dimension, and mesoscopic (up to tens of μm) in the other two (Palermo, 2013). Ideally, graphene is infinite scale of sp^2 carbon atoms flat sheets (Wang et al., 2013). In another words, graphene can be also describe as one atom layer of thick graphite. Giem and Novoselov (2007) state that graphene is also the basic building block for graphitic material of other dimensionalities as shown in Figure 2.1.

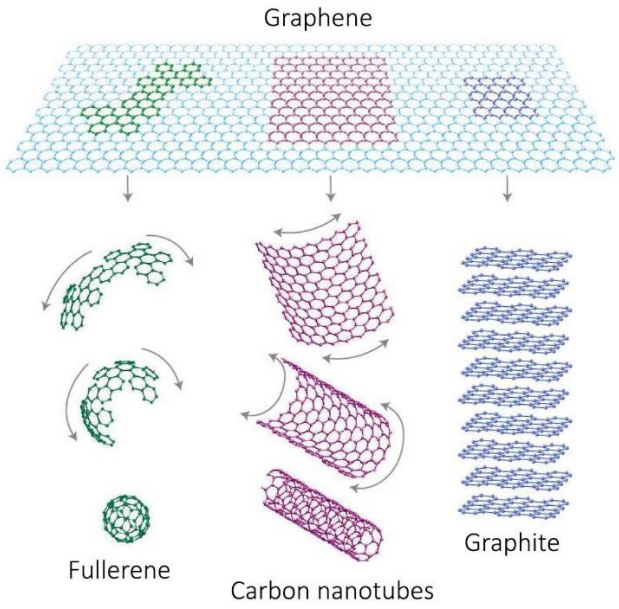

Figure 2.1: 2D graphene; 0D fullrenes; 1D carbon nanotube; 3D graphite (Geim and Novoselov, 2007)

The unique structure enables graphene possess many desired properties and promising applications. Graphene is a zero band gap semiconductor with giant carrier mobility of up to

200,000 cm^2/ (VS) (Novoselov et al., 2004). The optical transmittance of monolayer graphene can be as high as 98% (Novoselov et al., 2012). This leads graphene to become an excellent electronic material such as field emission transistors. In fact, the high aspect ratio and strong sp^2 C–C bonds of graphene give excellent mechanical properties. According to Lee et al. (2008) study, the intrinsic strength and Young's modulus of a single layer graphene has reported to be 130 GPa and 1.0 TPa respectively, by atomic force microscopy (AFM) measurement. A thermal conductivity of 5000 W/ (mK) has also been reported for graphene, which is 10 times higher than that of Copper (Cu) and superior to carbon nanotubes (CNTs) and diamond (Balandin et al., 2008). These distinctive properties have successfully attracted more and more research interest in using graphene and its derivatives as nano-fillers for composites (Stankovich et al., 2006).

2.2 Overview of Graphene Oxide (GO)

The oxidation product of graphene is known as graphene oxide (GO). GO is generally a single monolayer of graphene which has both aromatic regions (sp^2 carbon atoms) and oxygenated aliphatic regions (sp^3 carbon atoms) which contains hydroxyl, epoxy, carbonyl and carboxyl functional group in randomly distributed order (Georgakilas et al, 2012). Oxidation process breaks the π-π conjugation of sp^2 bonds and change to sp^3 bonds (Kim, Cote and Huang, 2010; Sheshmani and Amini, 2013). GO sheets have an apparent thickness of 1 nm and lateral size up to tens of micrometers. This gives GO sheets very large surface area (Kim, Cote and Huang, 2010). Figure 2.2 is a schematic model for GO sheet. The epoxy and hydroxyl functional groups are bound on the basal planes, while carboxyl groups are attached to the edges of the basal plane (Park et al., 2009).

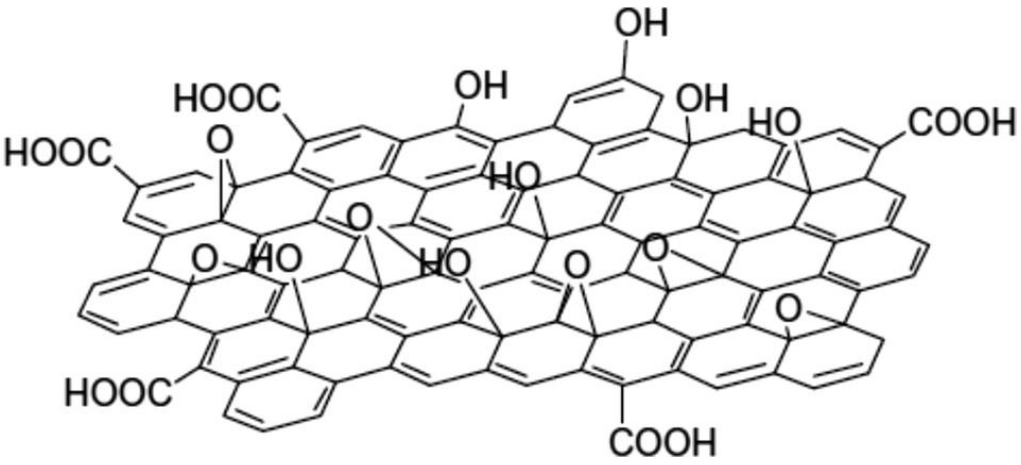

Figure 2.2: Schematic model of GO (Georgakilas et al., 2012)

The oxygen functional groups in the GO sheets induce the GO to be hydrophilic and it is ready to be exfoliated in water (Park et al., 2009). According to Park et al. (2009) research, the reactive oxygen functional groups also enable GO sheets to be chemically linked to other chemicals and substances.

Generally, GO is produced by the treatment of graphite using strong mineral acids and oxidizing agents, such as via treatment with $KMnO_4$ and H_2SO_4,as in the Hummers method or modified Hummers method, or $KClO_3$ (or $NaClO_3$) and HNO_3 as in the Staudenmaier or Brodie methods (Olanipekun et al., 2014). GO can be exfoliated using a variety of methods, most commonly by thermal shocking or chemical reduction in appropriate media, yielding a material reported to be structurally similar to that of pristine graphene on a local scale (Potts et al., 2011).

2.3 Overview of Reduced Graphene Oxide (rGO)

Reduced graphene oxide (rGO) is a reduction derivative of GO and is a process that converts sp^3 carbon to sp^2 carbon (Li et al., 2014).It is reported the electrical, thermal, mechanical properties and surface morphology of rGO and pristine graphene are similar. The precursor material for the production of rGO is primarily GO.

rGO can be prepared by various methods such as thermal exfoliation of graphite, chemical vapor deposition (CVD) and reduction of GO. Among these methods, chemical reduction of GO in organic solvents is more favorable due to its simplicity, reliability, suitability for large-scale production, low material cost, and versatility in chemical functionalization. (Tien et al., 2012).

Thermal exfoliation is by applying rapid heating to GO, yielding thermally expanded graphite oxide (TEGO). The rapid heating is believed to cause various small molecule species (e.g., CO, CO_2, water) to evolve and internal pressure to increase, forcing the sheets apart and yielding a dry, high-surface area material with a low bulk density (Zhao et al., 2014).This method is fast and eco-friendly as it does not require the use of any solvent or reducing agent. Moreover, due to the polar oxygen containing functional groups and the wrinkled nature, the thermally exfoliated rGO can be readily dispersed in polar organic solvent such as acetone. (Wen et al., 2014).

Chemical vapor deposition (CVD) is the most desired method for producing large area and high quality single or multilayer rGO using catalytic substrates and hydrocarbons (Karamat et al., 2015). The reaction occurs at moderate temperature. This method is the most common applied in producing nanocomposites coated with graphitic structure such as graphitic carbon nanotubes. It formed high purity products, allows the growth at large amount with reasonable cost (Atchudan et al., 2015).

Chemical reduction of GO is the most widely applied technique for preparing rGO by applying reducing agent such as hydrazine hydrate, hydroquinone, sodium borohydride and dimethyl-hydrazine (Li et al., 2014). This method yields large production of rGO at low cost. However, the reducing agents are mostly harmful to the environment and highly toxic (Zhang et al., 2010).

2.4 Preparation of Graphene Oxide

The main methods for oxidation of graphite include Brodie, Staudenmaier and Hummers-Offeman methods. These reactions are conducted under strong acid and strong oxidizer (Titelman et al., 2004).

B. C. Brodie method of GO synthesis was the first method developed in 1859 by reacting slurry of graphite in fuming nitric acid (HNO_3) with potassium chlorate ($KClO_3$). The net empirical formula of the graphene after successful oxidation is $C_{2.19}$ $H_{0.80}$ $O_{1.00}$ (Dreyer et al., 2009).

Later, L. Staudenmaier modified and improved Brodie's method. Staudenmaier's modified the method by adding chlorate in multiple aliquots over the course of reaction. Besides that, concentrated sulphuric acid (H_2SO_4) was added to increase the acidity of the mixture. This modification is more practical as the reaction can take place in a single reaction vessel.

Generally, both method practices using nitric acid and potassium chlorate as the oxidizing agent. HNO_3 is known to be common oxidizer and can react strongly with aromatic carbon surface and releases NO_2 or N_2O_4 during the reaction. $KClO_3$ is known to be strong oxidizer which is commonly used in explosive materials (Dreyer et al., 2009). It is relatively dangerous and hazardous. Typical result of reaction often yields formation of oxygen containing species such as ketones, carboxyls and lactones (Dreyer et al., 2009).

In 1957, Hummers and Offeman developed another method of oxidation of graphene by using the combination of potassium permanganate ($KMnO_4$) and concentrated sulphuric acid (H_2SO_4). The reaction is said to be less hazardous, time saving, ease in fabrication and popular compare to the other two.

Equation 2.1 shows the formation of dimanganese heptoxide (Mn_2O_7) formed from the reaction of potassium permanganate and sulfuric acid. According to Dreyer et al. (2010), Mn_2O_7 was the active species of the oxidant although permanganate was a well establish oxidising agent. The bimetallic heptoxide was more reactive than its monometallic tetraoxide counterpart (MnO_4^-). Therefore, Mn_2O_7 had a higher ability to oxidize graphite to GO. It tends to donate when the temperature was heated up to 55 ℃ and above. Temperature control is very important for this approach.

$$KMnO_4 + 3H_2SO_4 \rightarrow K^+ + MnO_3^+ + H_3O^+ + 4HSO_4^-$$
$$MnO_3^+ + MnO_4^- \rightarrow Mn_2O_7$$

Equation 2.1: Formation of dimanganese heptoxide (Dreyer et al., 2009)

On the other hand, many modifications have been proposed especially for Hummers method. Modification includes pre-expansion step of graphene prior to oxidation is believed to rise the degree of oxidation. This pre-treatment was done by reacting graphene with concentrated H_2SO_4, $K_2S_2O_8$ and P_2O_5. In 2010, modified Hummers method was published by Marcono et al. (2010). This method excluded the use of $NaNO_3$ and increasing the amount of $KMnO_4$. A mixture of H_2SO_4 and phosphoric acid (H_3PO_4) in 9:1 volume ratio was used. This method is said to increase yield without generate the toxic gas such as NO_2 or N_2O_4. Figure 2.3 shows several synthesis method of graphite oxide derived from Hummers method.

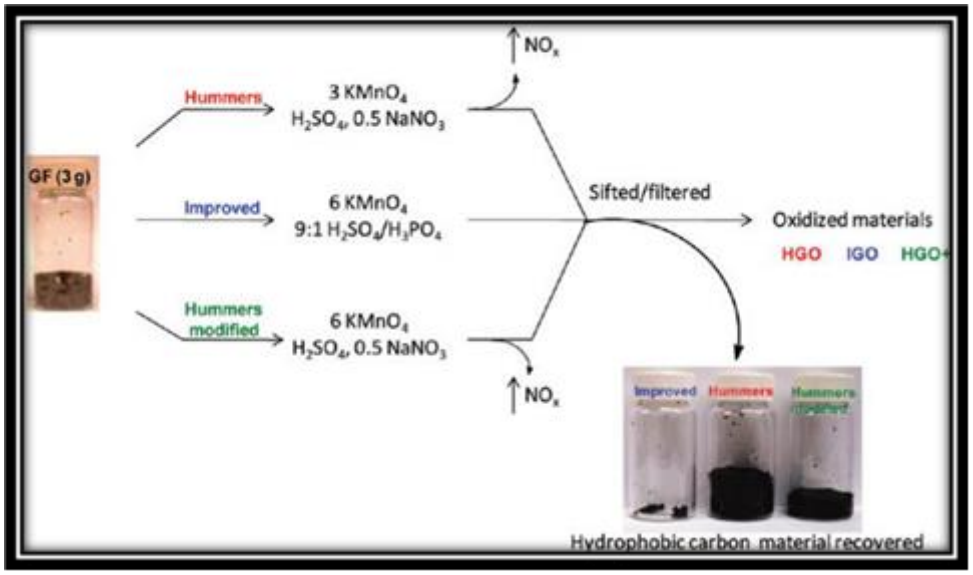

Figure 2.3: Synthesis method of GO (Marcano et al., 2010)

The post-treatment of graphite oxide includes elimination of reaction by the use of hydrogen peroxide. The product will undergo a series a washing to remove the impurities as well as to remove the sulphate ions with the use of hydrochloride acid. The solution is centrifuged and washed until the pH of the supernatant in neutral. The graphite oxide is then exfoliated fully in water through ultrasonification to obtain GO. The final product is then obtained by air drying or oven drying (Ganesh et al., 2013).

2.5 Reduction of Graphene Oxide

2.5.1 Thermal Reduction

First of all, reduction of GO can be done by thermal annealing reduction. In the early stages of graphene research, rapid heating (>2000 ℃/min) was usually used to exfoliate graphite oxide (Wu et al., 2009). The rapid heating has caused the CO or CO_2 gases evolved into the spaces between graphene sheets. The rapid heating not only exfoliates graphite oxide but also reduces the functionalized graphene sheets by decomposing oxygen- containing groups at elevated temperature. However, this method only can produce small size and wrinkled graphene sheets (Schniepp et al., 2006).The main reason is the decomposition of oxygen-containing groups also removes carbon atoms from the carbon plane, which splits the graphene sheets into small pieces and results in the distortion of the carbon plane, as shown in Figure 2.4.

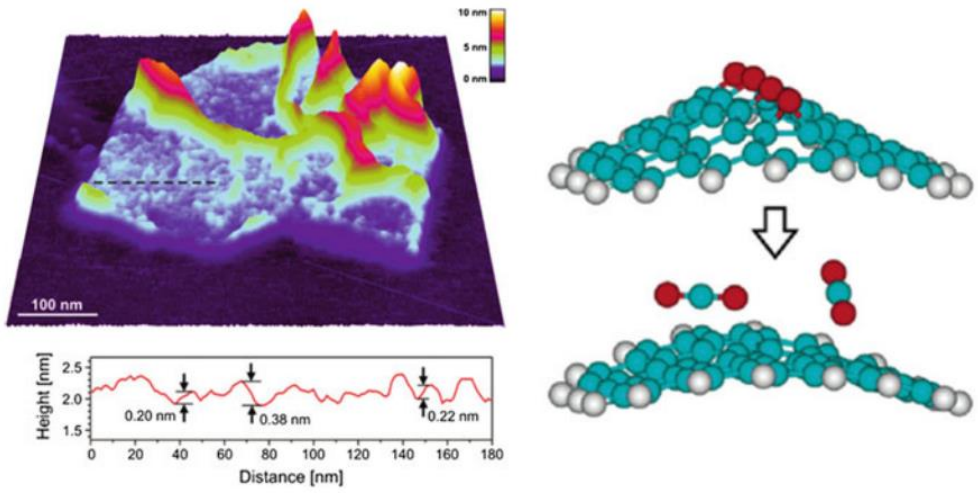

Figure 2.4: Pseudo-3D representation of a 600 nm × 600 nm AFM scan of an individual graphene sheet showing the wrinkled and rough structure of the surface, and an atomistic model of the graphite oxide to graphene transition (Schniepp et al., 2006)

Zhao et al., (2010) in the other hand had exfoliated graphite oxide in the liquid phase to form exfoliated graphene sheets with large lateral sizes. After the formation of macroscopic materials such as films and powders, the reduction is carried out by annealing in inert or reducing atmospheres. Schniepp et al. (2006) found that if the temperature was less than 500 ℃, the C/O ratio was no more than 7, while if the temperature reached 750 ℃, the C/O ratio could be higher than 13. Li et al. (2009) have monitored the chemical structure variation with

annealing temperature, and the XPS spectrum for the samples are shown in Figure 2.5. The results have showed that high temperature is needed to achieve good reduction of GO.

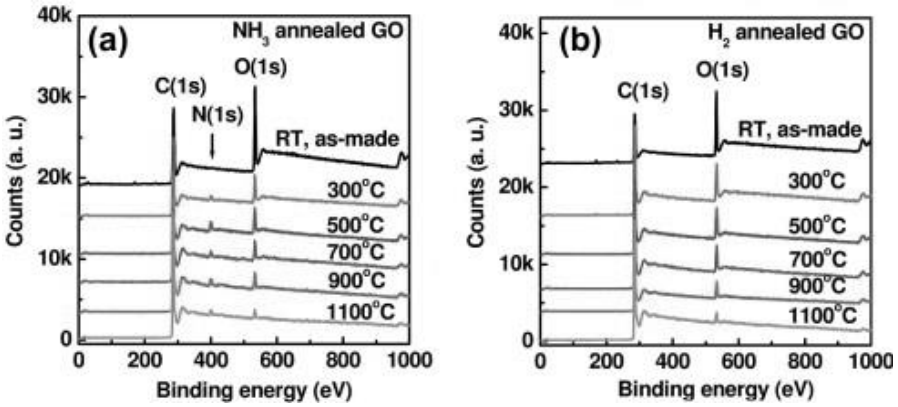

Figure 2.5: XPS spectra of GO sheets annealed in 2 Torr of (a) NH_3/Ar (10% NH_3) and (b) H_2 at various temperatures (Li et al., 2009)

Wang et al. (2009) has annealed GO thin films at different temperatures as shown in Figure 2.6. The results showed that the volume of electrical conductivity of the reduced GO film obtained at 500 ℃ was only 50 S/cm, while for those reduced at 700 ℃ and 1100 ℃ it could be 100 S/cm and 550 S/cm, respectively. Wu et al. (2009) used arc-discharge treatment to exfoliate graphite oxide to prepare graphene. Since the arc-discharge could provide temperatures above 2000 ℃ in a short time, the typical sheet electrical conductivity of graphene sheets was about 2000 S/cm, and elemental analysis revealed that the exfoliated graphene sheets had a C/O ratio of 15–18.

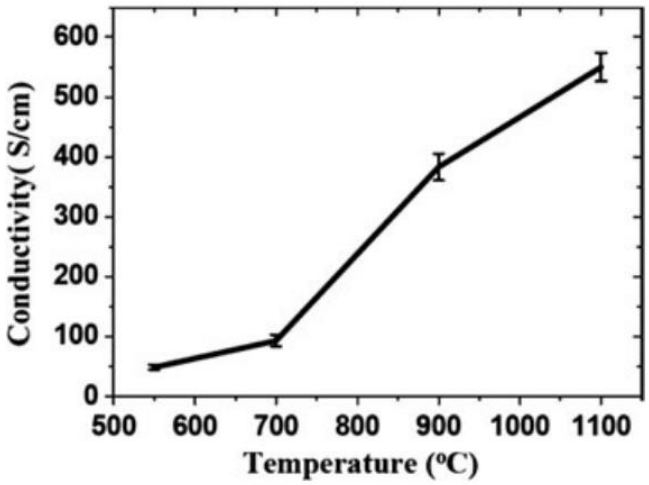

Figure 2.6: Increase of the average conductivity of graphene films from 49, 93, 383 to 550 S/cm, along with the temperature increasing from 550 ℃, 700 ℃, 900 ℃ to 1100 ℃, respectively (Wang et al., 2009)

In fact, some unconventional heating resources such as microwave irradiation (MWI) and photo irradiation have been used to exfoliate GO. The MWI can heat the substances uniformly and rapidly. rGO can be obtained within 1 min in ambient conditions by MWI method (Zhu et al., 2010). Unlike conventional thermal heating, MWI allows better control of the extent of GO reduction by hydrazine hydrates due to the MWI power and time can be adjusted to yield a nearly complete reduction of GO. The occurrence of non-equilibrium local heating of GO will cause formation of hot spots (electric discharge) in the rGO, which could lead to the development of structural defects in the graphene lattice. These defect sites act as nucleation centers for the formation of the metal nanoparticles, which can be anchored to the graphene sheets.

2.5.2 Chemical Reduction

Reduction of GO can be also carried by using chemical reagent. This method is based on the reagent's chemical reactions with GO and could be done at room temperature or moderate heating. Thus, this method is a cheaper and easier way for the mass production of graphene as compared to thermal reduction.

The used of hydrazine to reduce GO was first reported by Stankovich et al. (2007) The reduction by hydrazine and its derivatives such as hydrazine hydrate and dimethylhydrazine, can be achieved by adding the liquid reagents to a GO aqueous dispersion which results in agglomerated graphene-based nanosheets due to the increase of hydrophobility. When dried, an electrically conductive black powder with C/O ratio around 10 can be obtained. (Stankovich et al., 2007). The highest conductivity of rGO films produced solely by hydrazine reduction is 99.6 S/cm combined with a C/O ratio of around 12.5 (Fernandez-Merino et al., 2010).

In organic chemistry, metal hydrides, e.g. sodium hydride, sodium borohydride ($NaBH_4$) and lithium aluminium hydride are known as strong reducing reagents. However, these reducing agents have reactivity with water, which is the main solvent for the exfoliation and dispersion of GO. Shin et al. (2009) has reported that $NaBH_4$ was more effective than hydrazine as a reducing agent of GO. Although it is also slowly hydrolyzed by water, its use is kinetically slow enough that the freshly-formed solution functions effectively to reduce GO. As an improvement, Gao et al. (2012) proposed an additional dehydration process using concentrated sulphuric acid (98 % H_2SO_4) at 180 ℃ after reduction by $NaBH_4$ to further improve the reduction effect on GO. The C/O ratio of rGO by the two-step treatment is about 8.6 and the conductivity of the rGO powder produced is about 16.6 S/cm.

Fernandez-Merino et al. (2010) reported that ascorbic acid (Vitamin C: VC) is a new reducing reagent for GO, which is considered to be an ideal substitute for hydrazine. The report revealed that GO reduced by VC could achieve a C/O ratio of about 12.5 and a conductivity of 77 S/cm, which are comparable to those produced by hydrazine in a parallel experiment. In addition, VC has great advantage of its non-toxicity in contrast to hydrazine and a higher chemical stability with water than $NaBH_4$. Furthermore, the reduction in colloid state does not result in the aggregation of rGO sheets as produced by hydrazine, which is beneficial for further applications.

2.5.3 Electrochemical Reduction

Reduction of GO can be done by electrochemical removal of oxygen functionalities (Zhou et al., 2009). Electrochemical reduction of GO sheets or films can be carried out in a normal electrochemical cell using an aqueous buffer solution at room temperature. Normally, there is no special chemical agent needed. The reduction is mainly caused by the electron exchange between GO and electrodes. Therefore, this could avoid the use of dangerous reducing agent such as hydrazine and eliminate by- products.

After depositing a thin film of GO on a substrate, an inert electrode is placed opposite the film in an electrochemical cell and reducing occurs during charging of the cell. By cyclic voltammetric scanning in the range of 0 to −0.1 V (respect to a saturated calomel electrode) to a GO-modified electrode in a 0.1 M KNO3 solution, Ramesha et al. found that the reduction of GO began at −0.6 V and reached a maximum at −0.87 V. The reduction can be achieved by only one scan and is an electrochemically irreversible process in this scanning voltage range.

Zhou et al. (2009) found out electrochemical method gives the best reduction effect. The report revealed that rGO produced could achieved a C/O ratio of 23.9, and the conductivity of the rGO film produced was measured to be approximately 85 S/cm. They found that the potential needed to realize the reduction is controlled by the pH value of the buffer solution. A low pH value is preferable to reduce GO.

2.6 Natural Rubber (NR)

Natural rubber (NR) was originally derived from latex by the addition of acetic or formic acid. It is a linear polymer of an unsaturated hydrocarbon called isoprene (2-methyl butadiene). Figure 2.7 shows the chemical structure of NR.

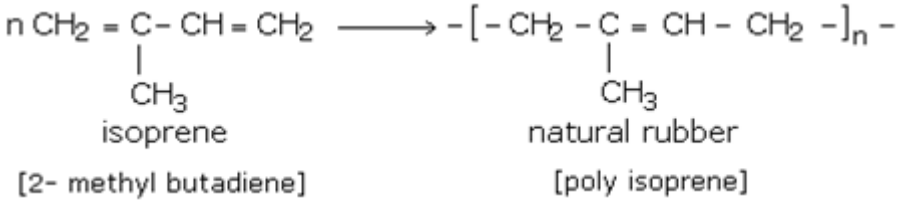

Figure 2.7: Structure of natural rubber (Tutorvista.com, 2015)

The molecular weights of rubber molecules range from 50,000 to 3,000,000. 60% of the molecules have molecular weights of more than 1,300,000. The repeating unit in NR has cis configuration which is essential for elasticity. If the NR has trans configuration, the polymer is either a hard plastic that used for modern golf ball covers.

Crude rubber is a tough and an elastic solid. It becomes soft and sticky as the temperature rises. It has a specific gravity of 0.915. It absorbs large quantities of water. It is insoluble in water, alcohol, acetone, dilute acids and alkalis. However, it is soluble in carbon disulphide, carbon tetrachloride, petrol and turpentine. Pure rubber is an amorphous solid, which on stretching or prolonged cooling becomes crystalline.

The most important property of NR is its elasticity and flexibility. However, raw NR has low tensile strength and abrasion resistant and only has elasticity over a narrow range of temperature from 10 to 60 ˚C. Charles Goodyear discovered the process of vulcanization in 1893 to modify the properties of NR (Kohjiya and Ikeda, 2014). The sulfur cross-linking of NR is shown in Figure 2.8.

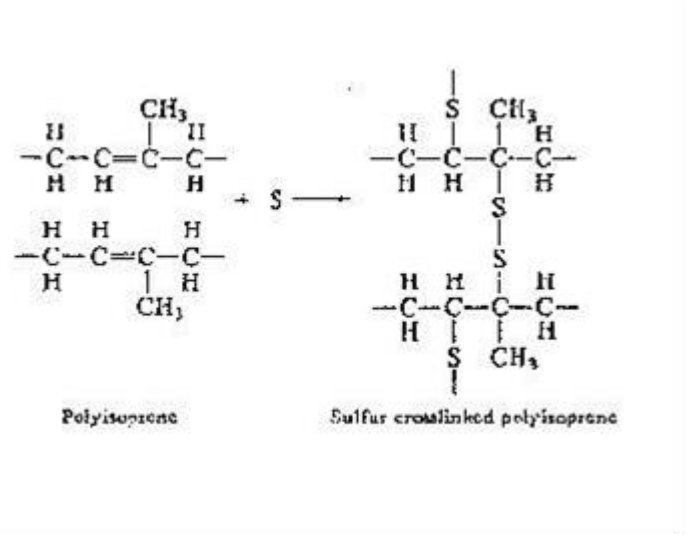

Figure 2.8: Sulfur cross-linking of natural rubber (Tutorvista.com, 2015)

Vulcanization is a process where a certain amount (5-8 %) of sulfur is added to the NR to form crosslinking between the molecular chains. The double bonds in NR permit formation of sulfur bridges between different chains. These cross-links are responsible for removing the tackiness of untreated rubber. Vulcanized NR will exhibit several properties such as higher elasticity, tensile strength and resistance to abrasion. Additives such as carbon black, clay, talc and calcium carbonate can be added into the NR while compounding to improve its properties (Groover, 2010).

2.7 Natural Rubber Composites

There are few previous studies on natural rubber composites. Xu et al., (2015) had used epoxidized natural rubber (ENR) as an interfacial modifier to improve the mechanical and dynamical mechanical properties of NR/silica composites. (ENR) is a modified rubber prepared by epoxidized reaction of NR in peroxycarboxylic acid. The modulus, tensile strength, tear strength and wear resistance of NR/silica composites were improved after the modification with ENR. The improvement of the properties can be attributed to the ring-opening reaction between the epoxy groups of ENR chains and Si-OH groups on the silica surface.

Oil palm ash (OPA), could also be used as a filler to be compounded with NR (Ooi et al., 2014). Based on the studies, the tensile strength was improved. However, the researchers found out the tensile strength could be further enhanced by surface treatment of OPA with Liquid Epoxidized Natural Rubber (LENR). The OPA is compounded with NR and other curing ingredients, using a laboratory two-roll mill. After being subjected to thermal ageing at 100 ˚C for two days, the tensile strength and elongation at break of the LENR-coated OPA filled NR composite showed higher retention than non-coated OPA filled NR composites. Thermogravimetric Analysis (TGA) indicated that the thermal stability of LENR-coated OPA filled NR composites was higher than that of non-coated OPA filled NR composites (Ooi et al., 2014).

On the other hand, polypyrrole (PPy)/NR blends were prepared by polymerizing pyrrole in NR latex using anhydrous ferric chloride as oxidizing agent (Promila Devi et al., 2013). Based on the studies, the PPy/NR composites show increased tensile strength, modulus and tear resistance.

2.8 Natural Rubber Nanocomposites

Nanocomposites have attracted many attention in recent years because of their diverse nanometer-sized filler particles and a series of special performance. NR/cellulose nanocomposites had been studied by Ortiz- Serna et al., (2014). The samples with filler content from 10phr to 30phr with thickness around 0.25 mm were studied under dielectric spectrometer. The interactions between the filler particles and the NR matrix slightly influence the electrical conductivity of the NR/cellulose nanocomposites. Cellulose nanoparticles maintain the inherent good dynamic properties of NR without sacrificing the insulating properties in applications where the lowest possible level of conductivity is desired.

Palygorskite-cerium oxide/ NR nanocomposites was prepared by Zhao et al., (2014). Palygorskite (PA)-cerium oxide (CeO_2) was modified with cetyl-trimethylammonium bromide (CTAB) to be used as filler to produce high-performance NR nanocomposites. The organic-modification of PA-CeO_2 led to good compatibility with the NR matrix. The mechanical properties of the nanocomposites were significantly improved.

Another example of NR nanocomposites is the montmorillonite (MMT) clay/NR with intercalation of fatty acids prepared by Ketiperachchi et al., (2012). Intercalation of fatty acids was done in an internal mixture which yielded expanded organo-montmorillonite (EOMt). Mixing of NR with different amounts of EOMt clay was done in an open two-roll mixing mill at 90 ℃. The larger interlayer space in the presence of fatty acid promoted the exfoliation of clay minerals in NR matrix.

2.9 Graphene Based Polymer Composites

In last two decades, nanomaterials have attracted tremendous attention as reinforcement for polymer matrix composites. Polymer nanocomposites can result in significant improvement in physical and mechanical properties at much lower loadings than polymer composites with conventional fillers. The discovery of graphene has created a new class of polymer nanocomposites due to its exceptional reinforcement in composites.

Chemically modified graphene/ polyaniline (PANI) nanofiber composites was prepared by in situ polymerization of aniline monomer in presence of GO in acidic medium (Zhang et al., 2010). Then, hydrazine monohydrate was used to reduce the resulting PANI/GO composites to a graphene composite. After that, the reduced PANI undergo reoxidation and reprotonation to form PANI/graphene nanocomposite. The conductivity of the PANI/graphene composites was 168.7 Sm^{-1}, which was slightly lower than that of PANI/GO composites of 231.2 Sm^{-1}. This may probably due to a decrease in the degree of doping in PANI, and a change in the morphology of the composites during the reduction, reoxidation and reprotonation process (Das et al., 2013).

Wang et al. (2009) prepared epoxy/graphene composites by using in situ polymerization and their electromagnetic interference (EMI) shielding were examined. The results showed that EMI shielding effectiveness increased with increasing graphene loading. Therefore, epoxy/graphene composites can be used as effective lightweight shielding materials for electromagnetic radiation. Furthermore, GO sheet-incorporated epoxy composites was prepared and thermal expansion was examined by a thermo-mechanical analyser (Kuilla et al., 2009). The epoxy resin has very poor thermal conductivity but the inclusion of graphene sheets showed a significant improvement of thermal conductivity. It was reported that 5 wt% GO-filled epoxy resin showed four times higher thermal conductivity than that of the neat epoxy resin (Yu et al., 2008). Thus, graphene composites act as a promising thermal interface material for heat dissipation.

A study of polyvinyl alcohol (PVA)/ graphene nanocomposites was conducted by incorporating GO into the PVA matrix (Liang et al., 2009). Water was used as the solvent for solution casting of the nanocomposites. The mechanical performance of PVA/ graphene nanocomposite was greatly improved than pure PVA. On the other hands, Zhao et al. (2014) prepared fully exfoliated graphene nanosheet/ PVA nanocomposites using a facial aqueous

solution. The mechanical behavior and tensile strength of the nanocomposite was enhanced with addition of graphene.

2.10 Preparation of Graphene Nanocomposites

The preparation method depends on the polarity, molecular weight, hydrophobicity and reactive groups present in the polymer, graphene and solvent (Zhang et al., 2010). There are three methods for incorporating graphene into the polymers; in situ intercalative polymerization, solution intercalation and melt intercalation.

2.10.1 In Situ Intercalative Polymerization

Firstly, graphene or modified graphene is swollen within the liquid monomer. A suitable initiator is added and polymerization is initiated by heating or radiation (Zheng et al., 2004). There are several graphene nanocomposites have been prepared using this method, such as polystyrene (PS)/ graphene (Zheng et al., 2004), polymethylmethacrylate (PMMA)/ expanded graphite (EG) (Chen et al., 2003) and polyaniline (PANI)/graphene (Zhang et al., 2010) nanocomposites. In situ polymerization achieves a high level of dispersion of graphene-based filler without prior exfoliation. Although the polymerization may exfoliate the graphite nanoplatelets (GNPs), single-layer graphene platelets were not observed (Fim et al., 2010). In situ polymerization technique makes possible the covalent bonding between the functionalized sheets and polymer matrix via various chemical reactions. The main disadvantage of this technique is the increase of viscosity with the progress of polymerization process that hinders manipulation and limits load fraction. Another drawback is the process sometimes may need to carry out in the presence of solvents. Thus, the removal of solvent is a critical issue similarly in the solvent mixing technique (An et al., 2011).

2.10.2 Solution Intercalation

Solution mixing is the most straightforward method for preparation of polymer composites. In this method, graphene or modified graphene layers are allowed to swell and the polymer is soluble in the solvent system (Stankovich et al., 2006). Firstly, graphene or modified graphene is dispersed in a suitable solvent like water, acetone, chloroform, tetrahydrofuran (THF), dimethyl formamide (DMF) or toluene. After that, the polymer is adsorbed onto the delaminated sheets and finally the solvent is evaporated (Lee et al., 2007). There are a wide range of graphene nanocomposites have been prepared using this method like polyethylene-grafted maleic anhydride (PE-g-MA)/ graphite (Hussain et al., 2006), polystyrene (PS)/ graphene (Wanga et al., 2004), polypropylene (PP)/ graphene (Kalaitzidou et al., 2007), polyvinyl alcohol (PVA)/ graphene (Liang et al., 2009) nanocomposites. The solvent

compatibility of the polymer and the filler plays an important role to achieve good dispersion. However, solvent removal is a critical issue.

2.10.3 Melt Intercalation

In this method, graphene or modified graphene is mixed with the polymer matrix in molten state. A thermoplastic polymer is mixed mechanically with graphene or modified graphene at elevated temperatures using conventional methods like extrusion and injection molding (Wanga et al., 2006). The graphene or modified graphene are then intercalated or exfoliated in the polymer matrix to form nanocomposites. Graphene nanocomposites such as polypropylene (PP)/ expanded graphite (EG) (Kalaitzidou et al., 2007), high dense polyethylene (HDPE)/ EG (Kim et al., 2009), polyphenylene sulphide (PPS)/ EG (Chen et al., 2003) and polyamide (PA6)/ EG (Weng et al., 2005) nanocomposites have been prepared by this method. Relative to solution intercalation, melt intercalation is more economical because no solvent is used. However, this method is less effective in dispersing graphene in the polymer matrix especially at higher filler loadings due to increased viscosity of the nanocomposites (Kim et al., 2010). Another drawback of this technique is buckling, rolling or even shortening of graphene sheets during mixing due to strong shear forces which is not favourable for better dispersion (An et al., 2011).

CHAPTER 3

METHODOLOGY

3.1 Materials/ Reagents

In view of the conventional Hummers methods, GO was prepared from the graphite nanofiber (GNF) and other chemicals. Ultrapure deionized water (DI) was used throughout the process and can be obtained in UTAR PE lab.

The materials and reagents used were as following: graphite nanofiber (GNF) was supplied by Platinum Senawang Sdn Bhd. sulphuric acid (H_2SO_4, 95 %), hydrochloric acid (HCl, 37 %) and hydrogen peroxide (H_2O_2, 30 %) were obtained from R&M Chemicals. Sodium nitrate ($NaNO_3$), potassium permanganate ($KMnO_4$) were purchased from Bendosen Laboratory Chemicals and hydrazine hydrates was supplied from Sigma-Aldrich Co. LLC. Standard Malaysian Rubber grade 10 (SMR 10), zinc oxide (ZnO), stearic acid, BKF (antixodant, 2,2'-Methylene-bis-[4-methyl-6-tert-butylphenol]), rubber vulcanization accelerator (CBS), sulphur were provided by Universiti Sains Malaysia. All chemicals were analytically pure and were used as received.

3.2 Preparation of Graphene Oxide (GO)

Conventional Hummers method was used for the synthesis of GO in this experiment. The experimental set up for the preparation of GO was shown in Figure 3.1.

Initially, 5.0 g of graphite GNF was added into a 500 ml beaker loaded with 115 ml of sulphuric acid (H_2SO_4). Then, the beaker was placed under an overhead stirrer to provide homogeneous stirring at 400 rpm. An ice bath was prepared and used to maintain the temperature of beaker and reaction at 0 ˚C. Next, 2.5 g of sodium nitrate ($NaNO_3$) was added into the beaker.

After the $NaNO_3$ dissolved, 15.0 g of potassium permanganate ($KMnO_4$) was added gradually over 30 minutes to counteract overheating of the reaction mixture (<30 ˚C). Then, a visible green suspension formed almost instantaneously.

Figure 3.1: Experimental set up for preparation of GO

After 10 minutes of stirring, the ice bath was removed and the temperature of the mixture was brought up to approximately 35 ˚C. Subsequently, a purplish vapour was observed and formed as the mixture was heated up. Then, the solution was stirred vigorously at 500 rpm for duration of 3 hours at room temperature (Figure 3.2).

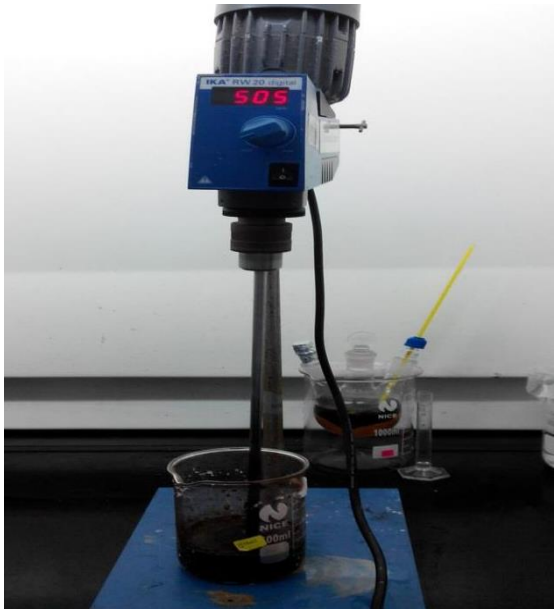

Figure 3.2: Solution stirred at 500 rpm for 3 hours at room temperature

After 3 hours, the speed of stirrer was reduced to 400 rpm and a dark brown solution was formed. Meantime, 230 ml of ultrapure deionized water (DI) was prepared and added slowly into the solution. There was a large exothermic reaction occurred when the water was added. The temperature of the mixture increased significantly to 70 ˚C and was maintained until the water was completely added into the solution.

The mixture was then stirred for another 10 minutes and added into 700 ml of ultrapure deionized water. Next, 12 ml of hydrogen peroxide (H_2O_2) was added in order to reduce the residual $KMnO_4$, resulting a light yellow suspension of graphene oxide formed. After that, the mixture was left overnight in the fume hood (Figure 3.3) and was filtered using the Whatman Anodisc membrane on the next day.

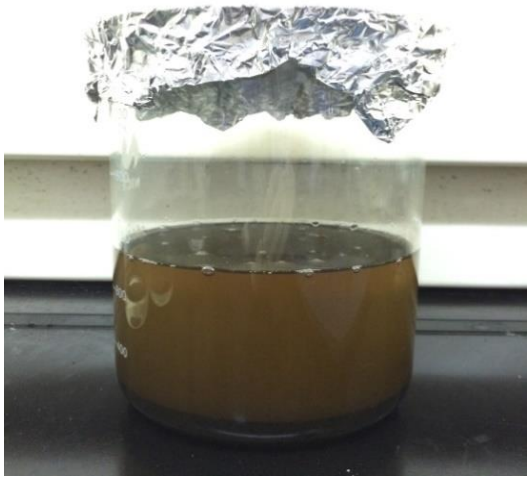

Figure 3.3: GO solution left overnight

Then, the filtered cake obtained was washed with 5 % HCl aliquots solution, followed by deionized water for several times. The washing was carried out using decantation of supernatant with centrifugation with 10,000 rpm for 20 minutes at room temperature. Finally, the pH of the supernatant was tested with pH paper and when it reached approximately in between the range of 5 to 7, the product was dispersed in deionized water and dried overnight in an oven at around 60-80 ˚C.

3.3 Preparation of Reduced Graphene Oxide (rGO)

First of all, 500 mg of GO was dispersed in 500 mL of deionized water and then exfoliated by ultrasonication (100 W) for 1 hour. Subsequently, 5mL of 99 % hydrazine hydrate was added, and the solution was heated in heating mantle with stirrer at 100 ℃ under a water-cooled condenser for 24 hour (Figure 3.4).

Figure 3.4: Solution heated in heating mantle with stirrer at 100 ℃ under a water-cooled condenser for 24 hour

After heating at 100 ℃, the solution turns from brown to black precipitate. The product was cooled, filtered, and washed with copious amount of deionized water by using manifold (Figure 3.5). Lastly, the product was dried at 60 ℃ under vacuum overnight to obtain rGO solid (Figure 3.6).

Figure 3.5: Product cooled, filtered and washed with copious amount of deionized water

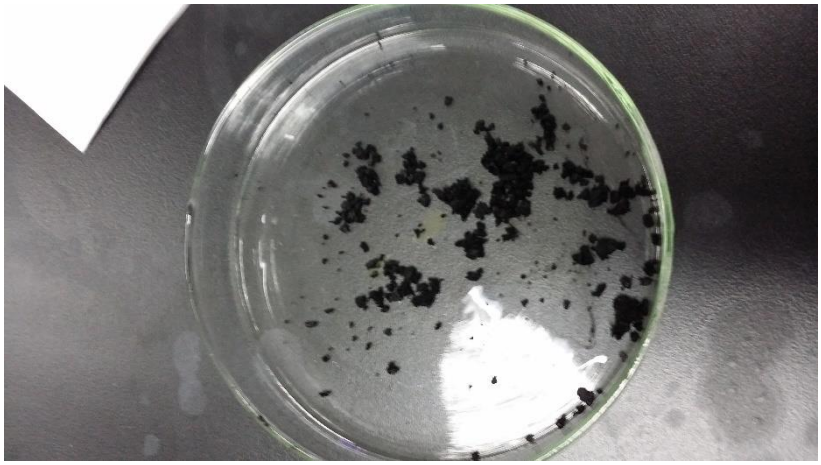

Figure 3.6: rGO solid obtained

3.4 Nanocomposites Preparation

3.4.1 Compounding

Natural rubber (NR) was first masticated on the laboratory open two roll mill (XK160) for ten minutes. Zinc oxide, stearic acid, sulphur and other rubber additives were added sequentially into the masticating NR (Figure 3.7). The compounds were prepared according to ASTM D3182 formulations as shown in Table 3.1. The appearances of NR compounds were as shown in Figure 3.8.

Table 3.1: Compound Formulation

	Compound (g)			
Ingredients	NR	NR/0.5 phr rGO	NR/1.0 phr rGO	NR/1.5 phr rGO
Natural Rubber	132.16	130.00	130.70	130.43
Zinc Oxide	6.61	6.49	6.60	6.52
Stearic Acid	3.96	3.90	4.41	3.91
BKF	1.30	1.30	1.30	1.30
CBS	2.64	2.60	2.71	2.61
Sulphur	3.30	3.25	3.40	3.27
Reduced Graphene Oxide	0	0.66	1.30	1.96

Figure 3.7: Natural rubber compounding in two roll mills

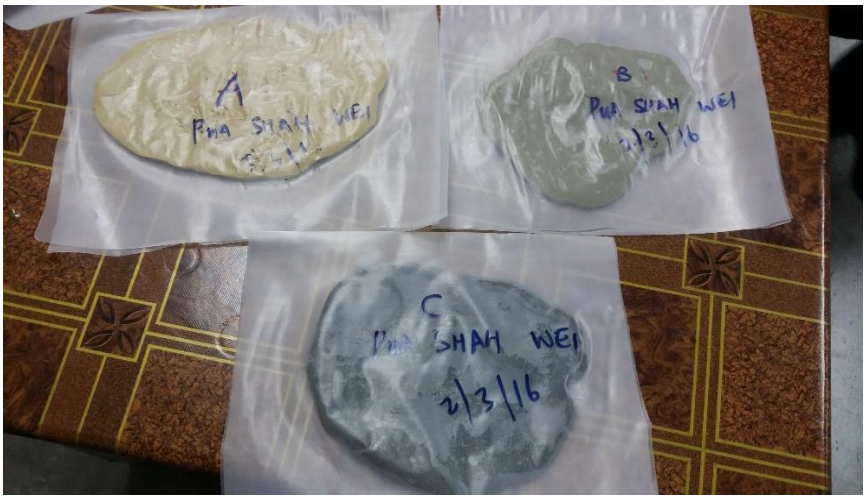

Figure 3.8: Natural rubber compounds

3.4.2 Rheometer Test

The curing of samples were carried out and the curing characteristics, cure time (t_{90}), scorch time (t_{S2}), minimum torque (ML), maximum torque (MH) and cure rate index (CRI) were determined using a Monsanto Moving Die Rheometer (MDR 2000) according to ASTM D2084 (Figure 3.9). Samples of respective compounds were tested at a vulcanization temperature of 150 ℃. Sheets of 2 mm thickness were compressed and molded at 150 ℃ ± 2 ℃ with 10 MPa force using a hot laboratory press at the respective cure time (t90) determined with the MDR 2000.

Formula for the calculation of CRI are based on Equation 3.1:

$$CRI = \frac{100}{cure\ time - scorch\ time} \quad \textbf{(3.1)}$$

Figure 3.9: Monsanto Moving Die Rheometer (MDR2000)

3.5 Characterization of Filler

3.5.1 Fourier Transform Infrared Spectrophotometer (FTIR)

FTIR (Nicolet photospectrometer 8700) was used to provide information on the chemical functional groups of the graphite nanofiber (GNF), graphene oxide (GO) and reduced graphene oxide (rGO). Potassium bromide (KBr) pressed pellet method was applied to analyze GNF, GO and rGO. Analysis was conducted to determine the absorption band with a wavelength range of 4000 cm^{-1} to 400 cm^{-1} with 4 scans at a resolution of 4 cm^{-1}.

3.5.2 X-ray Diffraction (XRD)

Siemens XRD Diffractometer 5000 was used to conduct XRD analysis with specular reflection mode at room temperature. Analysis of samples were performed in the scanning range of 2θ between 0˚ to 80˚ using nickel filtered copper Kα radiation (λ=0.154 nm) at a scan speed of 1 ˚/min. Interlayer spacing and crystalline structure of GNF, GO, rGO were recorded.

Bragg's Equation was used for the calculation of interlayer spacing based on Equation 3.2:

$$d = \frac{n\lambda}{2sin\theta} \quad \textbf{(3.2)}$$

where:

d = Interlayer Spacing (Armstrong)

λ = Wavelength

3.5.3 Thermal Gravimetric Analysis (TGA)

TGA (Mettler Toledo TGA SDTA851 E) was used to conduct TGA analysis to determine the thermal decomposition temperature of GNF, GO, rGO and the nanocomposites. All measurements were conducted under dynamic nitrogen flow over a temperature range of 35-800 ˚C at a heating rate of 10 ˚C/min.

3.5.4 Field Emission Scanning Electron Microscope (FESEM)

FESEM model JOEL JSM 6701F was used to conduct SEM analysis to determine the surface morphology of GNF, GO, rGO and the nanocomposites. The preparation of samples was carried out by coating the nanofillers with a thin layer of platinum. The analysis of GNF, GO and rGO were conducted with magnification of 20,000 X at 2.0 kV while the analysis of the nanocomposites was conducted with magnification of 300 X at 20.0 kV.

3.6 Performance Test

3.6.1 Tensile Test

Tensile test was carried out to determine the ultimate tensile strength, elastic modulus and percentage elongation at break of the nanocomposites. The tensile test was conducted using Tinius Olsen light weight tensile tester machine according to ASTM D412 test method using dumb-bell shaped test specimens at a uniform speed of 100mm/min. Tensile fracture surface was further examined under FESEM.

3.6.2 Hardness Test

The hardness of the nanocomposites was measured according to ASTM D2240 test method. The average value of readings taken at five different locations on each samples at room temperature was calculated.

3.6.3 Fatigue Test

The fatigue life of nanocomposites was tested using a Monsanto Fatigue To Failure Tester (FTFT) at 150 ℃. Individual dumbbell samples were cut by using a BS type E dumbbell cutter. The samples were then subjected to repeated cyclic strain at 100 rpm. The fatigue life in kilocycles (kc) for each sample was computed as the Japanese Industrial Standard (J.I.S) average, which was obtained from the four highest values using Equation 3.3.

The formula to calculate the fatigue life:

$$\text{J.I.S. average} = 0.5A + 0.3B + 0.1(C+D) \quad \textbf{(3.3)}$$

where A is the highest value, followed by B, C and D.

3.6.4 Swelling Test

Swelling behaviour of the nanocomposites was measured by the change in mass of samples under the exposure of toluene and n-hexane over a period of time. Samples were immersed in toluene and n-hexane under ambient temperature for 5 days. Next, samples were removed from the liquid and quickly wiped and weighted. The samples were further dried in an oven for 24 hours at temperature of 60 ℃. The dried samples were then cooled in a desiccator and weighted. The swelling parameters of respective nanocomposites were calculated and recorded using Equation 3.4 and 3.5.

Formulas to calculate the swelling parameters (Ahmed et al., 2012):

a) Mol % uptake (Qt)

$$Q_t\% = \frac{(w_1 - w_2)/w_2}{w_m} \times 100 \quad \textbf{(3.4)}$$

b) Swelling index (SI)

$$SI\% = (W_2 - W_1)/W_1 \times 100 \quad \textbf{(3.5)}$$

where:

W_1= initial weight

W_2= swollen weight

W_m= molar mass of solvent

CHAPTER 4

RESULTS AND DISCUSSIONS

4.1 Characterization of GNF, GO and rGO

4.1.1 Fourier Transform Infrared Spectroscopy (FTIR)

Figure 4.1 (a-c) represents the IR spectrum of GNF, GO and rGO. The absorption frequency regions and respective functional groups are tabulated in Table 4.1.

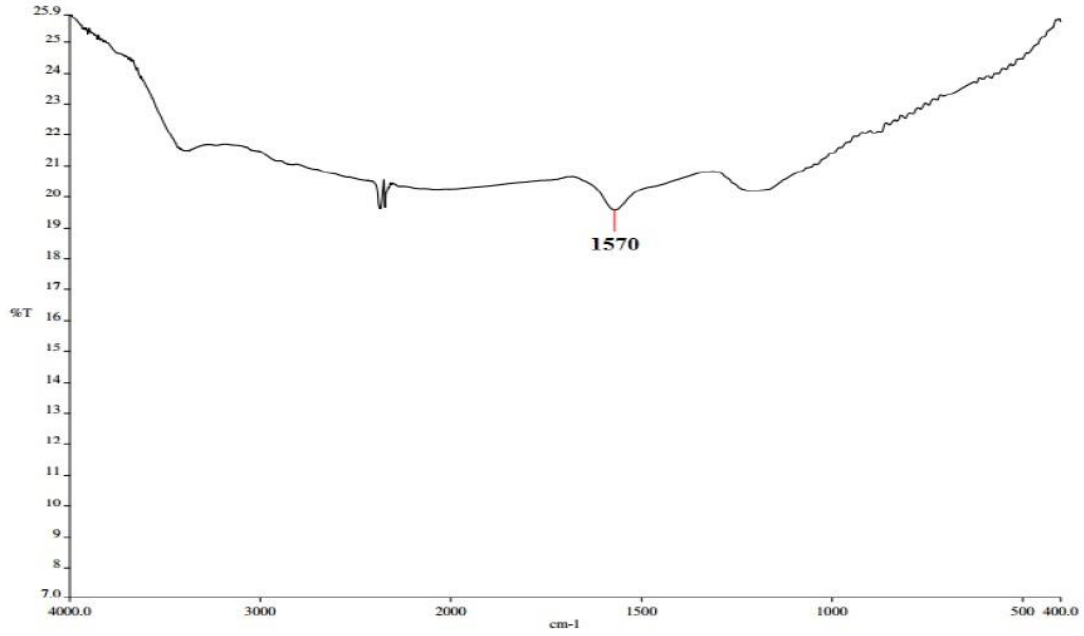

Figure 4.1(a): FTIR spectra of GNF

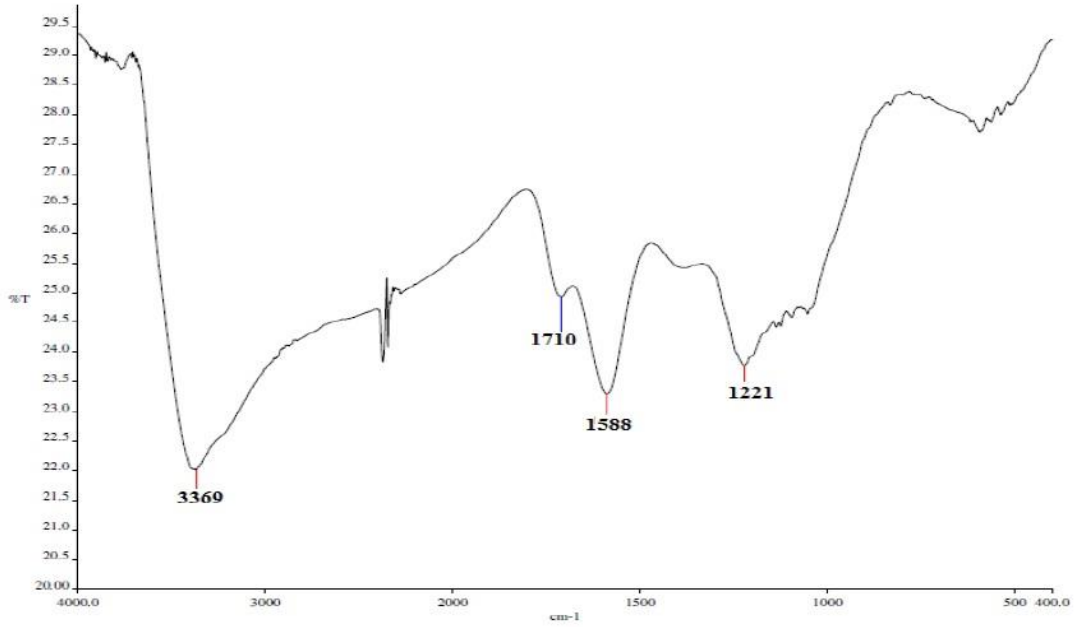

Figure 4.1(b): FTIR spectra of GO

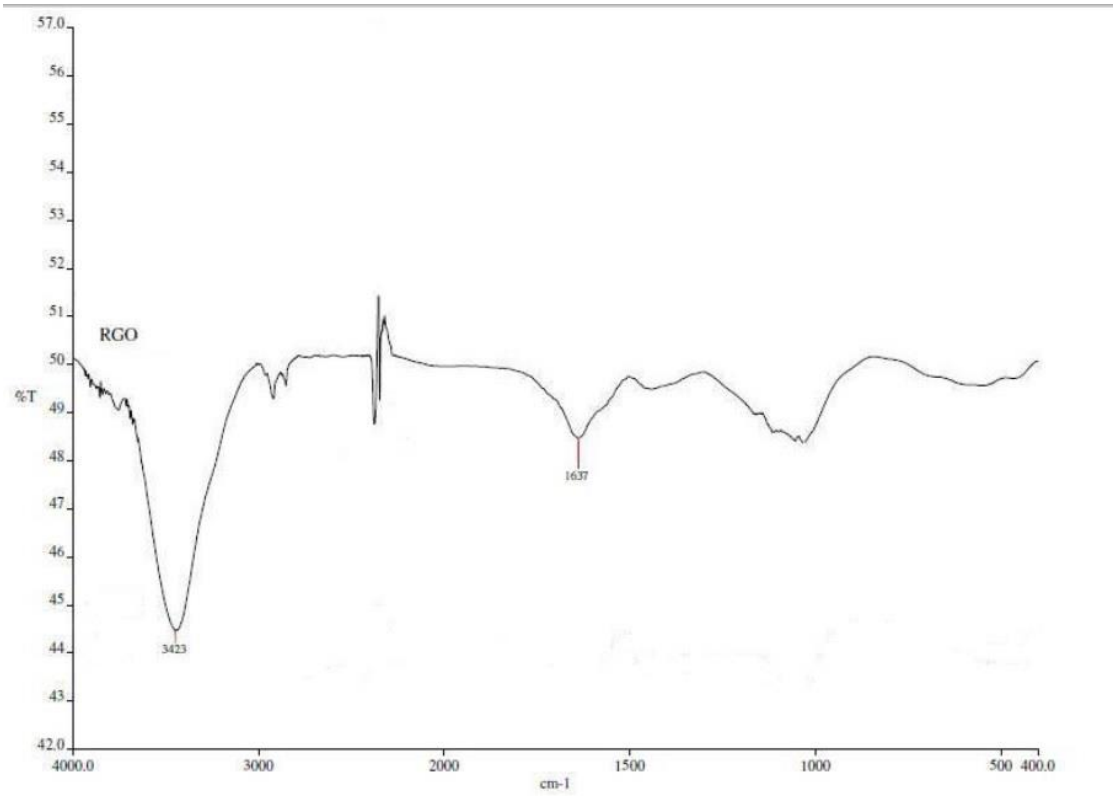

Figure 4.1(c): FTIR spectra of rGO

Table 4.1: Absorption frequency regions and respective functional groups

Absorption Frequancy (cm^{-1})	**GNF**	**GO**	**rGO**	**Bond**	**Functional Group**
3550-3200		3369	3423	O-H	Alcohol/Phenol
1780-1710		1710		C=O	Carboxylic
1750-1680				C=O	Carbonyl
1700-1500	1570	1588	1637	C=C	Aromatic
1320-1210		1221		C-O	Carboxylic
1260-1000				C-O	Alcohol
1240-1040				C-O-C	Epoxide

In Figure 4.1(a), the peak at 1570 cm^{-1} represents the presence of C=C bonds for GNF. In Figure 4.1(b), the presence of the peak at 1221 cm^{-1} may due to the vibration of C-O-C epoxide function groups or C-O stretching of alcohol or carboxylic acid. Another peak at 1588 cm^{-1} indicates the presence of un-oxidized C=C bonds in graphite oxide. At 1710 cm^{-1}, the peak indicates the stretching of C=O bonds while the peak at 3369 cm^{-1} signifies the stretching vibration of OH groups. The presence of oxygen- containing groups has proven that the GNF was oxidized to GO.

Peak at 1570 cm^{-1} in Figure 4.1(c) indicates the presence of C=C aromatic bond. Another peak at 3423 cm^{-1} was observed and this indicates the un-reduced OH bond. The C=O and C-O groups at 1710 cm^{-1} and 1221 cm^{-1} respectively were absence in Figure 4.1(c). This has proven the successful reduction of GO to rGO. Moreover, Tran et al., (2014) also reported similar absorption peaks for both GO and rGO.

4.1.2 X-ray Diffraction (XRD)

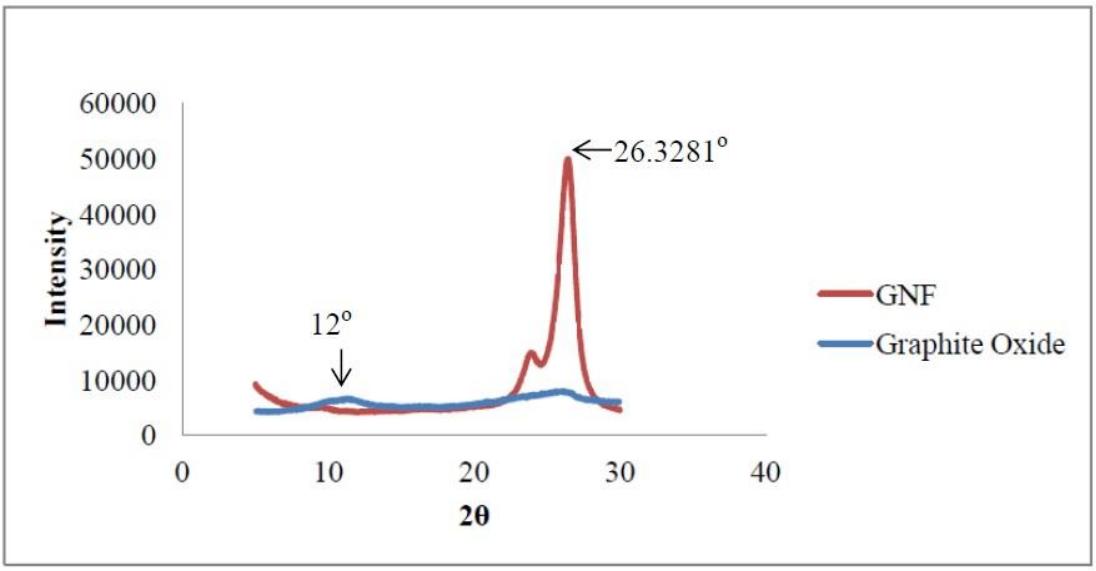

Figure 4.2: XRD diffraction data of GNF and GO

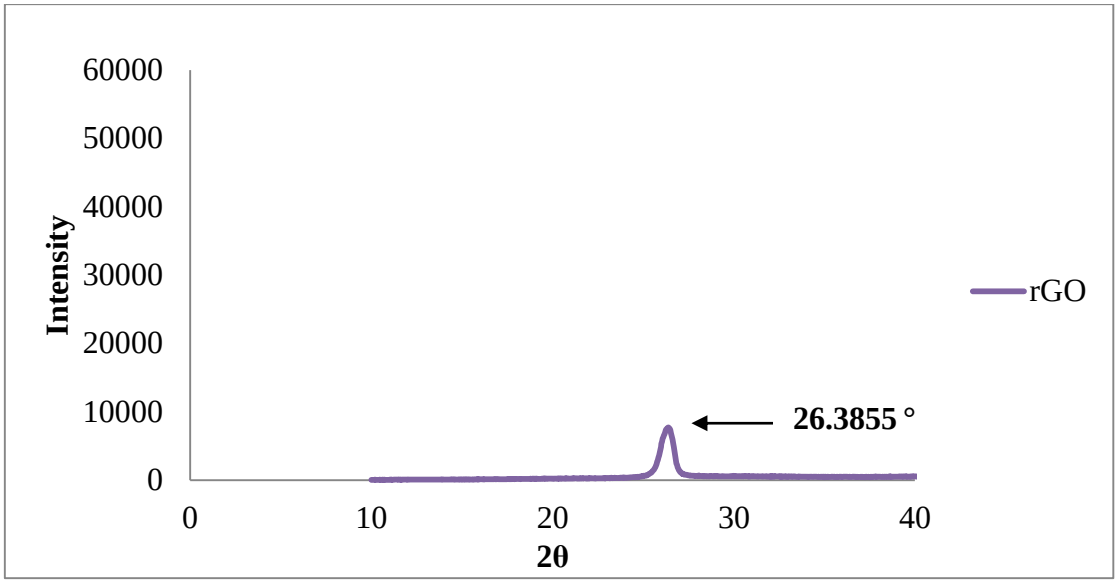

Figure 4.3: XRD diffraction data of rGO

Figure 4.2 shows the XRD diffraction data of GNF and GO while Figure 4.3 shows the XRD diffraction data or rGO. There is a peak of GNF at 2θ= 26.3281° represents to the spacing between the graphitic layers of 0.34 nm. However, graphene oxide shows a relatively very low peak, indicating successful oxidation of graphite where the introduction of oxygen functional groups increases interlayer spacing and caused exfoliation. Another small peak at 12 ° was observed for graphene oxide with an interlayer spacing of 0.74 nm. The increment of interlayer spacing is due to the presence of oxygen functionalities as it embedded into the layers. The

rGO, on the other hand, exhibits a new broad peak at 2θ= 26.3855°, with an interlayer spacing of 0.38 nm. This is because by the removal of oxygen functional groups, interlayer spacing will be reduced. A study conducted by Pendolino et al., (2015) also shown the similar diffraction peak.

4.1.3 Thermal Gravimetric Analysis (TGA)

The thermal stability of both GNF and GO were tested using TGA. Figure 4.4 shows the result obtained from TGA analysis of both GNF and GO whereas Figure 4.5 shows the result obtained from TGA analysis of rGO.

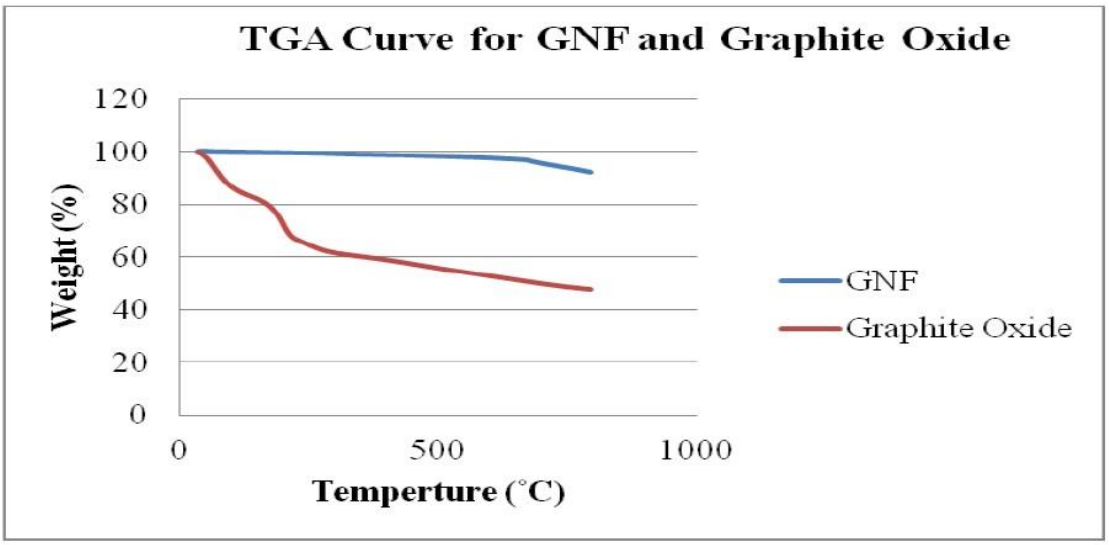

Figure 4.4: TGA curve for GNF and GO

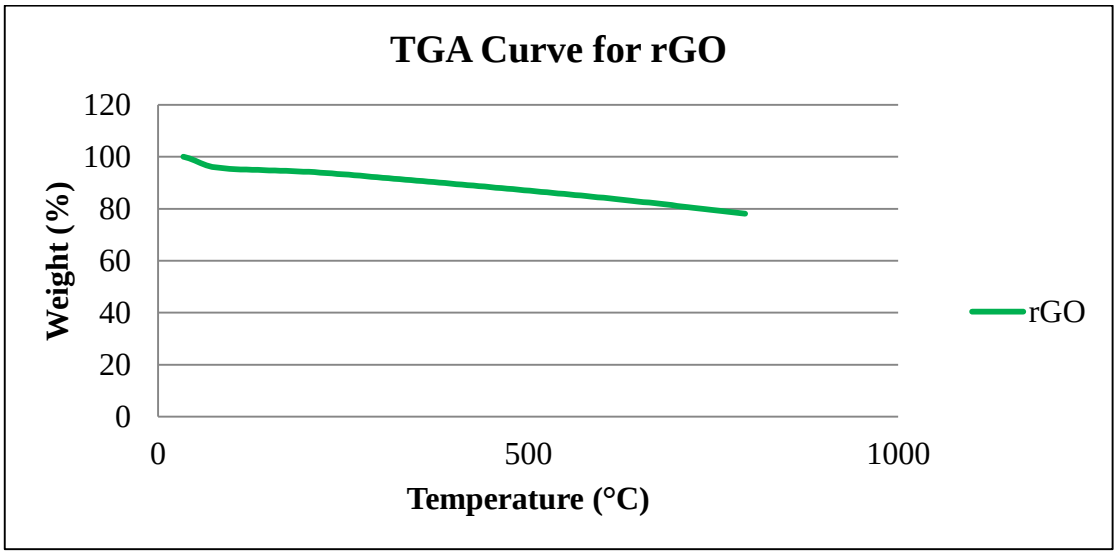

Figure 4.5: TGA curve for rGO

Pure GNF exhibited very high thermal stability due to the strong bonding between sp^2 hybridized carbons. As shown in Figure 4.4, the decrement in weight for GNF is insignificant up to the temperature around 680 ℃. The result was similar to the work done by Kumarasinghe et al., (2013). The total weight loss experienced by GNF when heated to temperature up to 800 ℃ was 7.9 wt%.

In contrast, GO exhibited weaker thermal stability. There were three weight loss regions for GO, as represented in Figure 4.4: below 100 ℃, 100-210 ℃ and 210-800 ℃ respectively. The weight loss found below 100 ˚C was due to the vaporization of intercalated water molecules. The second stage was due to the decomposition of functional groups. At the third stage, thermal decomposition continued at a slower rate. It is because most of the oxygen functional groups had been decomposed and subsequently left only the carbon backbones. Wang and Hu (2011) reported that most oxygen functional groups were removed at temperature below 240 ℃. The TGA results of GO indicates that the weight loss of GO are due to the loss of intercalated water, oxygen functional groups and carbon backbone. The total weight loss was about 52.5 wt%. RGO shows similar characteristic with GO while rGO has a lower amount of weight loss (21.9 wt%) as shown in Figure 4.5. This could be explained by the presence of a smaller amount of oxygen functional groups in the structure of rGO as compared to GO.

4.1.4 FESEM Analysis of GNF, GO and rGO

Figure 4.6 shows the micrographs of GNF, GO and rGO powders under FESEM with magnification of 20,000 X. From Figure 4.6(a), GNF shows coral tree-like structure. Figure 4.6(b) shows the structure of GO with a rougher surface. This is due to the presence of oxygen containing groups on the surface of graphitic layers. Similar results were reported by Zhao et al., (2014). Figure 4.6(c) shows a wrinkled paper-like structure of rGO. A study done by Silwana et al., (2015) had shown similar results.

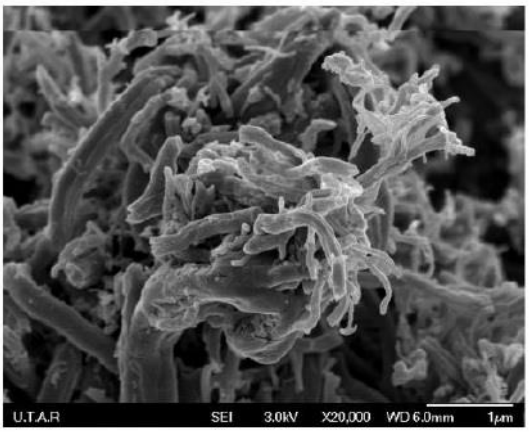

(a)

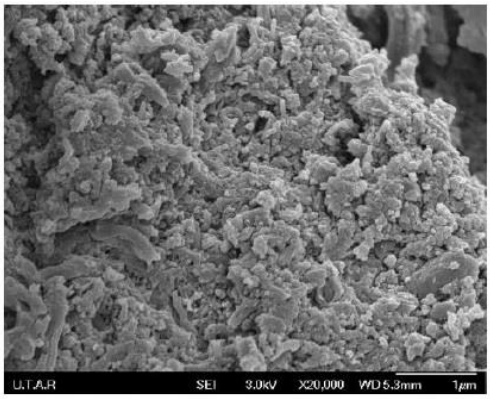

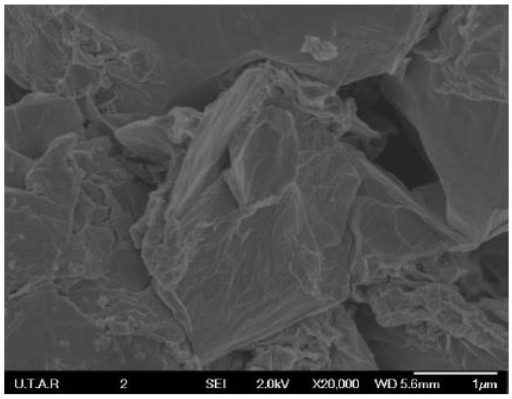

(b) **(c)**

Figure 4.6: FESEM micrographs at 20,000 X magnification of (a) GNF, (b) GO and (c) rGO

4.2 Rheometer Test

The curing properties of the nanocomposites are tabulated in Table 4.2.

Table 4.2: Curing properties of nanocomposites

Curing Properties	**Compound (g)**			
	NR	NR/ 0.5 phr rGO	NR/ 1.0 phr rGO	NR/ 1.5 phr rGO
ML (dNm)	0.06	0.05	0.00	-0.03
MH (dNm)	6.63	6.74	6.63	6.80
Torque Difference	6.57	6.69	6.63	6.83
t_{90} (min)	5.59	4.80	7.83	4.75
t_{S2} (min)	2.11	2.34	3.21	2.34
CRI	28.74	40.65	21.65	41.49

The obtained data shows that cures time (t_{90}) and scorch time (t_{S2}) of NR/1.0 phr rGO are the longest as compared to other nanocomposites. This may due to the presence of rGO content in nanocomposites which increase the relative site which require more time for cross linking in NR. Besides, CRI of NR/1.0 phr rGO nanocomposite is very similar to that of control NR and this enables NR/1.0 phr rGO nanocomposite to be applied without making changes to the process parameters.

Table 4.2 also shows that the increasing in rGO content in nanocomposites resulted in decreasing the minimum torque (ML). Besides, both NR and NR/1.0 phr rGO shared the lowest maximum torque (MH) of 6.63 dNm. It can be seen that the minimum torque which reflect the minimum viscosity of the nanocomposites is affected by the increasing rGO loading in the nanocomposites. A study conducted by Malas et al., (2012) had proposed a similar explanation.

4.3 Characterization of Nanocomposites

4.3.1 Thermal Gravimetric Analysis (TGA)

The thermal stability of all pure NR and the nanocomposites was investigated using TGA, the results of which are shown in Figure 4.7.

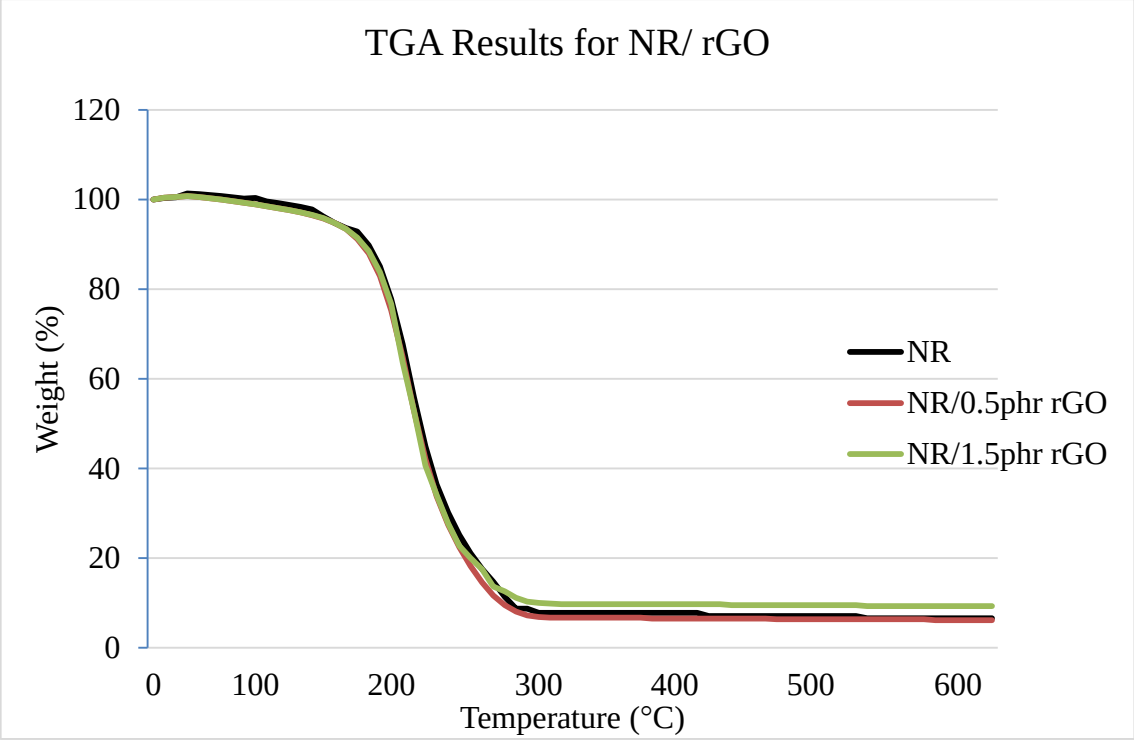

Figure 4.7: TGA curve of nanocomposites

Based on data obtained, the incorporation of rGO slightly enhanced thermal stability of nanocomposites. To assess the thermal stability, the temperatures corresponding to 5 % (T5 %) and 50 % (T50 %) weight loss of the nanocomposites were taken (Sahoo et al., 2009). There are no significantly differences in temperature T5 % for pure rubber (334.29 ℃) and all nanocomposites (334.84 °C for NR/0.5 phr rGO nanocomposites and 334.92 ℃ for NR/1.5 phr rGO nanocomposites). With the increase of rGO loading, the temperature T50 % of the nanocomposites is slowly increased from 393.67 ℃ for pure NR to 395.82 ℃ for NR/1.0 phr rGO nanocomposites. The T50 % for NR/1.5 phr rGO nanocomposites has also increased to 396.45 ℃. Moreover, rGO just like other layered materials such as clay and layered double hydroxides, creates the "tortuous path" effect, which act as barriers to prevent the permeation of oxygen and the escape of volatile degradation products from the sample. Furthermore,

presence of rGO also could facilitate the formation of strong char layer which could delay weight loss due to the decomposition (Huang et al., 2012).

4.4 Performance Test

4.4.1 Tensile Properties

Ultimate tensile strength, modulus and elongation at break of nanocomposites are recorded and shown in Figure 4.8- 4.11.

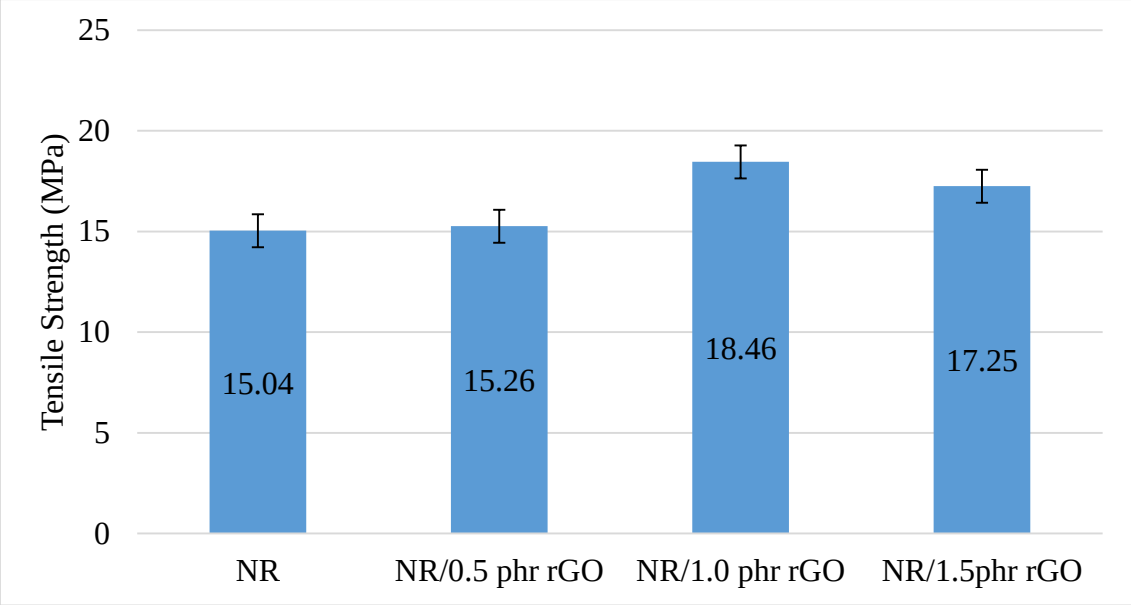

Figure 4.8: Ultimate tensile strength of nanocomposites

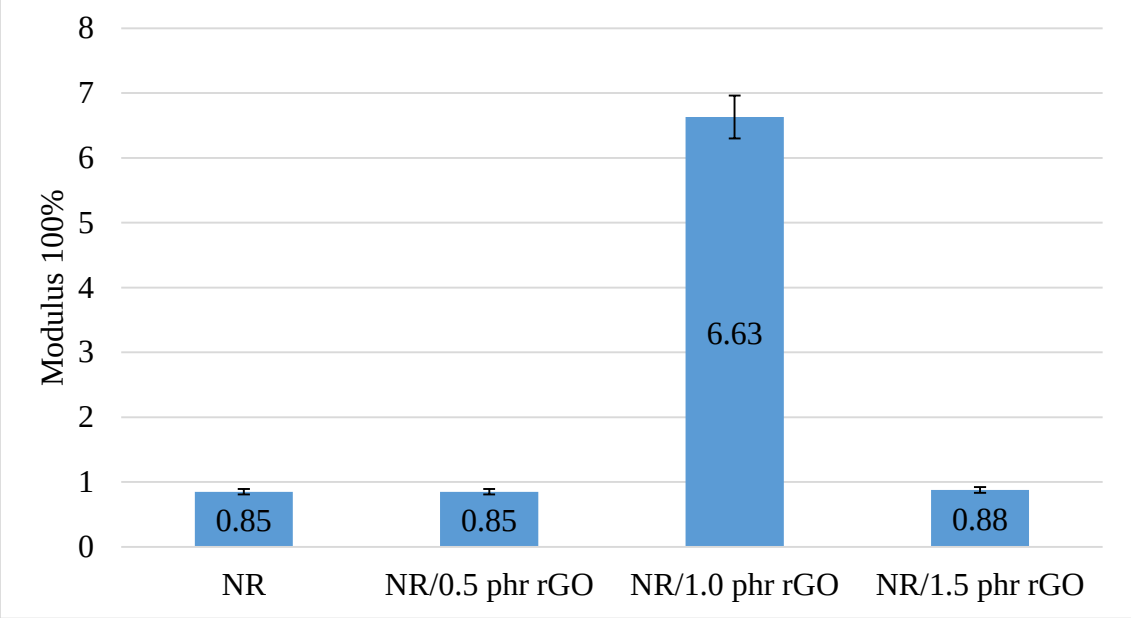

Figure 4.9: Modulus at 100% elongation comparison of nanocomposites

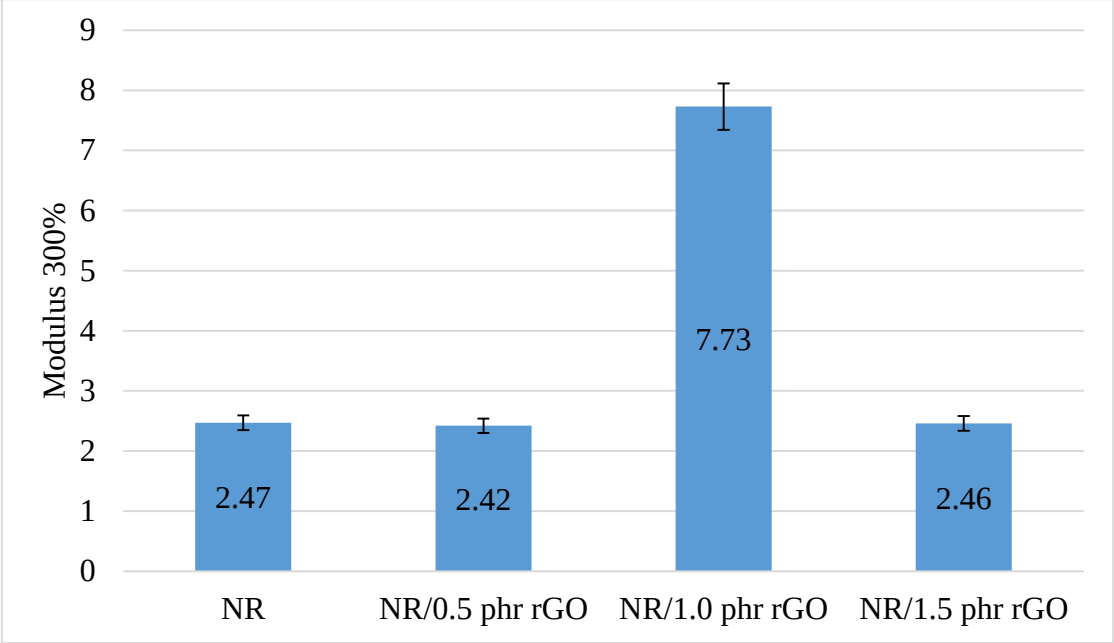

Figure 4.10: Modulus at 300% elongation comparison of nanocomposites

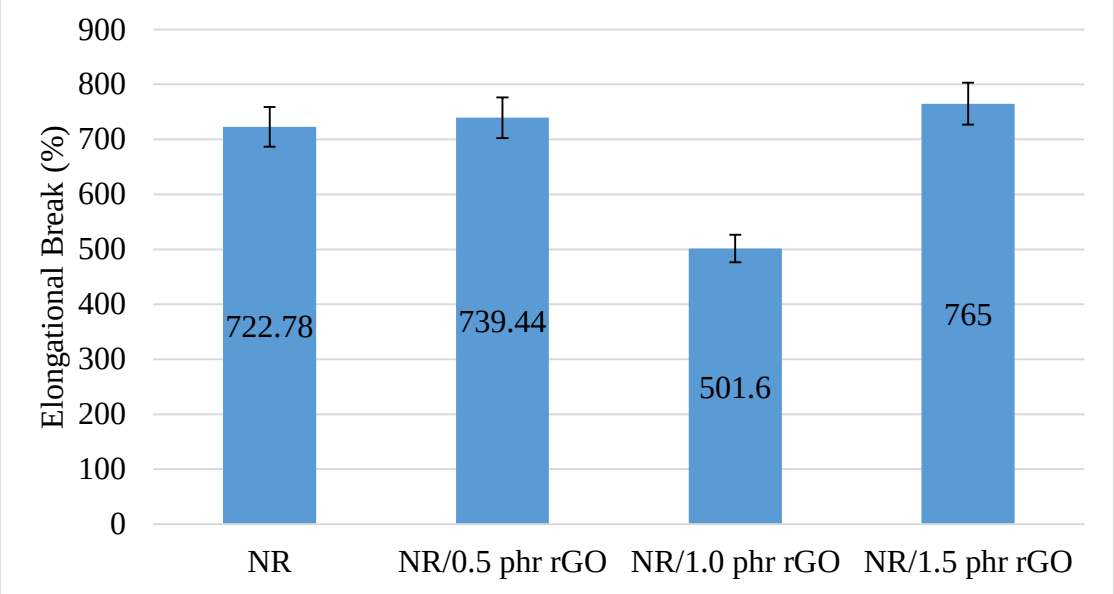

Figure 4.11: Percentage of elongation at break of nanocomposites

Figure 4.8 shows that increment in rGO loading resulted in increasing in tensile strength till 1.0 phr rGO. Then, the tensile strength was reduced in NR/1.5 phr rGO nanocomposites. It shows that the NR/1.0 phr rGO nanocomposites has the highest tensile strength of 18.46 MPa. Figure 4.9 and Figure 4.10 show the modulus at elongation of 100 % and 300 % respectively. NR/1.0 phr rGO nanocomposites show significant increase in modulus whereas the modulus of other compounds almost remained unchanged as compared to the control NR. Figure 4.11

shows the percentage of elongation at break (EB), NR/1.0 phr rGO nanocomposites has the lowest EB while the EB of the other two compound are almost the same as control NR.

Improvement of tensile strength in NR/rGO nanocomposite at 1 phr rGO loading is because there is better stress transfer between the filler and matrix at this loading. rGO able to disperse well and form better interaction with rubber matrix and form homogeneous system. Moreover, the modulus at both 100 % and 300 % elongation increases due to the delocalization of natural rubber chain on the surface of rGO which reduce the elasticity and increase stiffness.

However, NR/1.5 phr rGO nanocomposites shows a significant drop in tensile strength Agglomeration of rGO at this loading might be the reason. This could be further proven by FESEM images. Agglomerated rGO will turn out to become stress concentration points.

4.4.2 FESEM Analysis of Nanocomposites

Figure 4.12 (a-d) shows the micrographs of tensile fracture surfaces of pure NR, NR/0.5 phr rGO, NR/1.0 phr rGO and NR/1.5 phr rGO nanocomposites under FESEM with magnification of 300 X. From Figure 4.12(a), it was observed that the pure NR tensile fracture surface exhibit matrix tearing and ductile fracture surface. Figure 4.12(b) shows almost similar tensile fracture surface with slightly more matrix tearing. No agglomeration of rGO or formation of voids is observed.

NR/1.0 phr rGO nanocomposites was observed to exhibit has a rougher surface as shown in Figure 4.12(c). Agglomeration of fillers or void cannot be seen at all. In additions, step like appearances which indicates propagation of crack growth from major plane could be observed at this loading. This indicates good dispersion of rGO in the rubber matrix and lead to improvement in tensile strength and modulus of the nanocomposites.

Figure 4.12(d) shows the fracture surface of NR/1.5 phr rGO nanocomposites where agglomeration was observed. The agglomerates will act as the stress concentration points when force is applied and lead to the reduction of tensile strength and modulus.

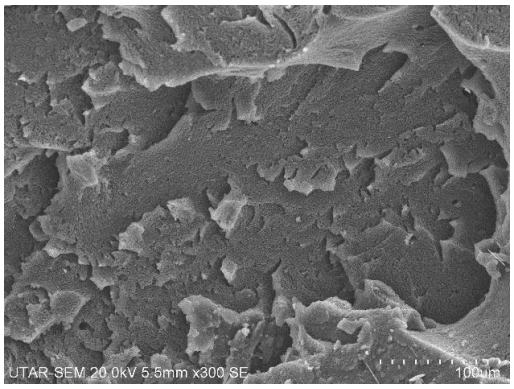

a)

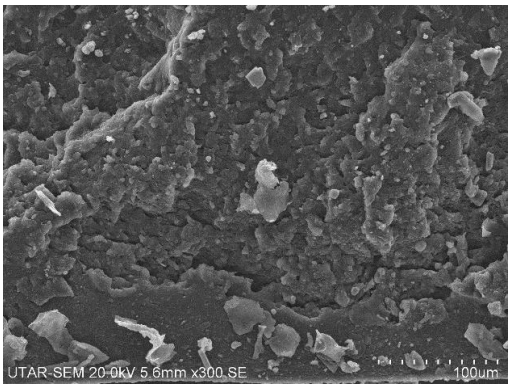

b)

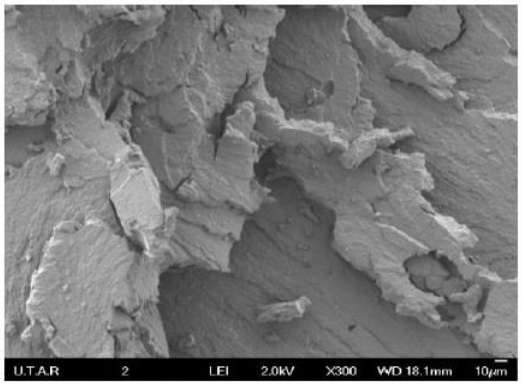

c)

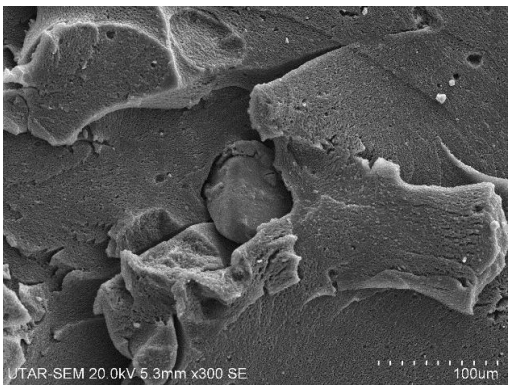

d)

Figure 4.12: FESEM micrographs at 300 X magnification of a) NR, b) NR/0.5 phr rGO, c) NR/1.0 phr rGO and d) NR/1.5 phr rGO nanocomposites

4.4.3 Hardness

Figure 4.13 shows the hardness of nanocomposites. Large improvement of hardness could be observed for NR/1.0 phr rGO nanocomposites. This is due to demobilisation of polymeric chain of the surface of the well dispersed rGO. NR/0.5 phr rGO did not show any improvement in hardness due to very low loading of filler; which will cause formation of non-homogenous system. While at 1.5 phr rGO loading agglomeration of rGO reduces the surface area for interaction and demobilization of polymeric chain.

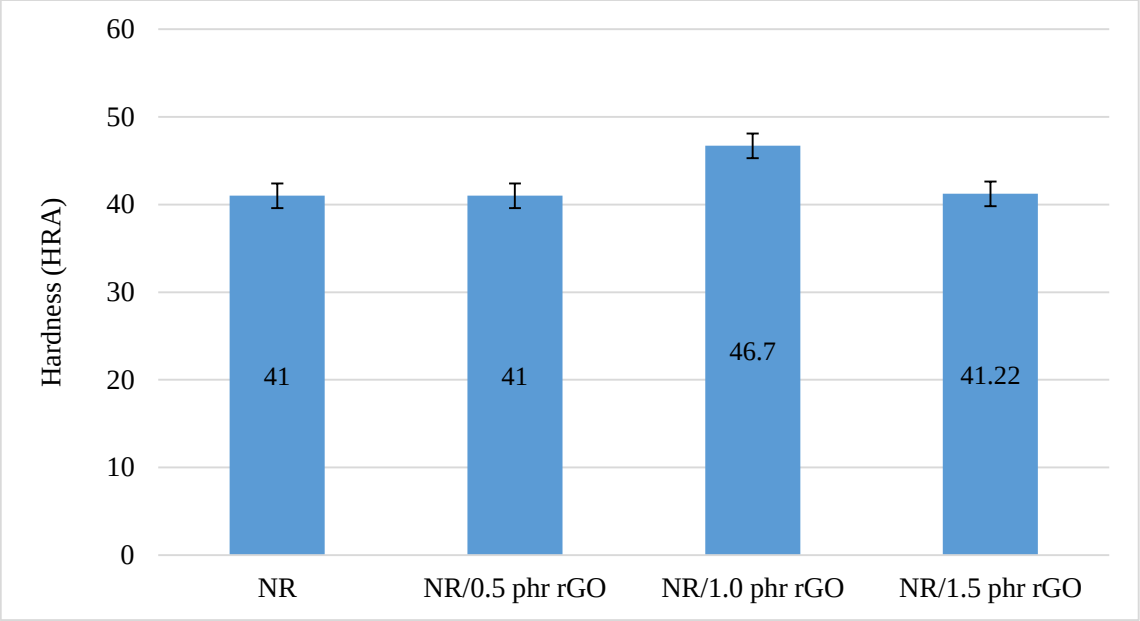

Figure 4.13: Hardness of nanocomposites

4.4.4 Fatigue Life

Figure 4.14 represents the dependence of fatigue life of natural rubber nanocomposites. The fatigue life of NR nanocomposites decreased noticeably as the filler loading increased (Figure 4.14). Similar fatigue life result was reported by Khanlari, S., (2011) using EOMt/ NR nanocomposites.

The unfilled NR compound exhibited the highest fatigue life value. This is because the ability of natural rubber to crystallize upon stretching. The strain induced crystallization have a beneficial effect on the fatigue fracture properties of rubber.

In Figure 4.14, the fatigue life of NR nanocomposites was reduced as the rGO loading increased. The decrement of fatigue life has proven the rGO has a significant effect on fatigue life. The reduction of the fatigue life of rGO filled NR nanocomposites is due to the heterogeneous nature of the nanocomposites. Thus, resulting in poor adhesion or incompatibility between polar rGO and non-polar NR. Therefore, crack growth resulting from filler agglomeration along with weak interfacial adhesion will lead to fatigue failure (Ismail et al., 2012).

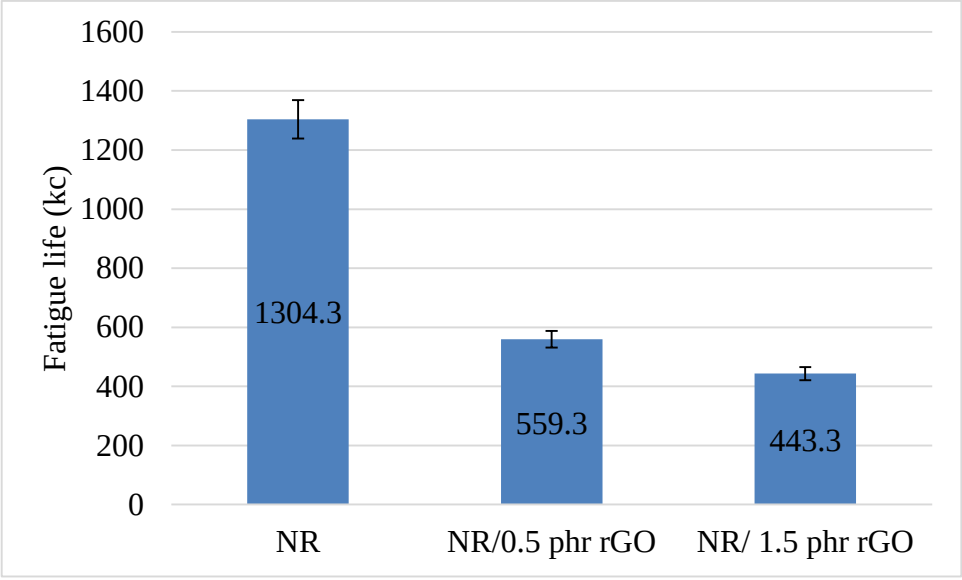

Figure 4.14: Fatigue Life of Nanocomposites.

4.4.5 Chemical Resistance

Table 4.3 illustrates the swelling parameter of nanocomposites. The swelling parameters indicates the chemical resistance for certain solvent of the nanocomposites. It was observed that all the NR/rGO nanocomposite shows significant reduction in Mol % uptake (Qt) and swelling index (SI) compared to control NR As Qt and SI reduced, the amount of solvent is able to penetrate into the nanocomposites also reduced. The obtained data also showed that NR/ 1.0phr rGO has the lowest Qt and SI. This is because 1.0phr rGO has the best dispersion which create tortuous path for solvent penetration. Hence, barrier layer is formed and resulting in more difficult for solvent to penetrate.

Table 4.3: Swelling Parameters

Solvent	Nanocomposites	Mol % Uptake (Qt)	Swelling Index (SI)
Toluene	NR	1.42	1.29
	NR/0.5 phr rGO	1.34	1.23
	NR/1.0 phr rGO	1.24	1.15
	NR/1.5 phr rGO	1.32	1.21
n-Hexane	NR	1.14	0.98
	NR/0.5 phr rGO	1.09	0.93
	NR/1.0 phr rGO	1.03	0.88
	NR/1.5 phr rGO	1.07	0.92

CHAPTER 5

CONCLUSION AND RECOMMENDATIONS

5.1 Conclusion

GO was produced through conventional Hummers method while rGO was produced through chemical reduction of GO. Characterization of GO and rGO has been conducted via FTIR, TGA, XRD and FESEM and it proves the oxidation and reduction of graphite.

Based on the research, NR/ 1.0phr rGO was the best nanocomposites to achieve the optimum properties. First, morphology study of the nanocomposites showed that only NR/1.0 phr rGO nanocomposite was having good dispersion in rubber matrix. Agglomeration occured when the rGO loading was at 1.5 phr. In fact, NR/1.0 phr rGO nanocomposite has the highest tensile strength of 18.46 MPa, modulus at 100 % elongation of 6.63 MPa, modulus at 300 % elongation of 7.73 MPa. It also showed the lowest elongation at break of 501.60 %. Furthermore, it has the highest hardness value of 46.7 HRA as compared to other nanocomposites. Chemical resistance study revealed that NR/1.0 phr rGO nanocomposite was having the highest chemical resistance with mol % uptake of 1.24 and 1.03 for toluene and n-hexane respectively. The Swelling Index were 1.15 and 0.88 for toluene and n-hexane respectively. Last but not least, the CRI of NR/1.0 phr rGO nanocomposite (21.65) was very similar to that of control NR (28.74) and this enabled NR/1.0 phr rGO nanocomposite to be process and crosslinked without making changes to the process parameters.

5.2 Recommendation

This study has demonstrated the enhanced mechanical and physical properties of NR/ rGO nanocomposites. The potential of rGO as a promising nanofiller in natural rubber has been proven. Besides, the optimum properties was obtained at 1.0phr rGO loading. Some steps can be carried out in order to optimise the process and properties of the nanocomposites.

- Determine suitable carrier such as dispersing agent that can be incorporated to further enhance the dispersion of rGO in natural rubber matrix.
- Developed an environmentally friendly with low cost method to prepare rGO.

REFERENCES

Ahmed, K., Sirajuddin Nizami, S., Zahid Raza, N. and Shirin, K. 2012. Cure Characteristics, Mechanical and Swelling Properties of Marble Sludge Filled EPDM Modified Chloroprene Rubber Blends. *AMPC*, 02(02), pp.90-97.

An, X., Simmons, T., Shah, R., Wolfe, C., Lewis, K. M., Washington, M., Nayak, S. K., Talapatra, S. and Kar, S. 2010. Stable aqueous dispersions of noncovalently functionalized graphene from graphite and their multifunctional high-performance applications. *Nano Letters*., pp. 4295- 4301.

Arroyo, M., López-Manchado, M. A., Herrero. B. 2003. Organo-montmorillonite as substitute of carbon black in natural rubber compounds. *Polymer,* 44 (8), pp. 2447–2453.

Atchudan, R., Perumal, S., Edison, T., Pandurangan, A. and Lee, Y. (2015). Synthesis and characterization of graphenated carbon nanotubes on IONPs using acetylene by chemical vapor deposition method. *Physica E: Low-dimensional Systems and Nanostructures*, 74, pp.355-362.

Balandin, A. A., Ghosh, S., Bao, W., Calizo, I., Teweldebrhan, D., Miao, F. 2008. Superior thermal conductivity of single-layer graphene. *Nano Lett.*, 8, pp. 902–907.

Bokobza, L. 2004. The reinforcement of elastomeric networks by fillers. *Macromol Mater Eng,* 289 (7), pp. 607–621.

Brownson, D. A., Kampouris, D. K. and Banks, C. E. 2011.An overview of graphene in energy production and storage applications. *Journal of Power Sources*, 196 (11), pp. 4873—4885.

Chen, G., Wu, D., Weng, W. and Wu, C. 2003. Exfoliation of graphite flakes and its nanocomposites. *Carbon,* 41, pp. 619–621.

Choi, W. and Lee, J. (2012). Graphene. *Boca Raton: CRC Press.*

Das, T. K. and Prusty, S. 2013. Graphene- based polymer composites and their applications. *Polymer- Plastics Technology and Engineering*, 52, pp. 319-331.

Dreyer, D. R., Park, S., Bielawski, C. W. and Ruoff, R. S. 2010. The chemistry of graphene oxide. *Chemical Society Reviews*, 39 (1), pp. 228—240.

Fernandez- Merino, M. J., Guardia, L., Paredes, J. I., Villar- Rodil, S., Solis- Fernandez, P., Martinez- Alonso, A. 2010. Vitamin C is an ideal substitute for hydrazine in the reduction of graphene oxide suspensions. *J Phys Chem C*, 114 (14), pp. 6426- 6432.

Fim, F. D. C., Guterres, J. M., Basso, N. R. S. and Galland, G. B. 2010. Polyethylene/graphite nanocomposites obtained by in situ polymerization. *J. Polym. Sci. Part A: Polym. Chem.*, 48 (3), pp. 692-698.

Ganesh, B., Isloor, A. M. and Ismail, A. 2013. Enhanced hydrophilicity and salt rejection study of graphene oxide-polysulfone mixed matrix membrane. *Desalination*, 313 pp. 199—207.

Gao, W., Alemany, L. B., Ci, L., Ajayan, P.M. 2009. New insights into the struction and reduction of graphite oxide. *Nat Chem*, 1 (5), pp 403- 408.

Gao, W. 2012. Graphite Oxide: Structure, Reduction and Applications.

Geim, A. K. and Novoselov, K. S. 2007.The rise of graphene. *Nature materials*, 6 (3), pp. 183—191.

Georgakilas, V., Otyepka, M., Bourlinos, A. B., Ch, Ra, V., Kim, N., Kemp, K. C., Hobza, P., Zboril, R. and Kim, K. S. 2012. Functionalization of graphene: covalent and non-covalent approaches, derivatives and applications. *Chemical reviews*, 112 (11), pp. 6156—6214.

Groover, M. 2010. Fundamentals of modern manufacturing. *Hoboken, NJ: J. Wiley & Sons*, pp.177, 178.

Gu, Z., Song, G., Liu, W., Li, P., Gao, L., Li, H. and Hu, X. (2009). Preparation and properties of styrene butadiene rubber/natural rubber/organo-bentonite nanocomposites prepared from latex dispersions. *Applied Clay Science*, 46(3), pp.241-244.

Hu, M. and Mi, B. 2013. Enabling graphene oxide nanosheets as water separation membranes. *Environmental science & technology*, 47 (8), pp. 3715—3723.

Huang, T, Lu, R. G., Su, C., Wang, H. N., Guo, Z., Liu, P., Huang, Z. Y., Chen, H. M. and Li, T. S. 2012. Chemically modified graphene/polyimide composite films based on utilization of covalent bonding and oriented distribution. *Appl. Mater. Interf*., 4, pp. 2699–2708.

Hussain, F., Hojjati, M., Okamoto, M. and Gorga, R. E. 2006. Review article, polymer–matrix nanocomposites, processing, manufacturing, and application, an overview. *J. Compos. Mater*, 40, pp. 1511–1575.

Ishak, Z. A. M., Abu Bakar, A., Ishiaku, U. S., Hashim, A. S., and Azahari, B. 1997. An investigation of the potential of rice hush ash as a filler for epoxidized natural rubber- II. Fatigue behaviour, *Euro. Polym. J*. 33, 73-79.

Ismail, H., Muniandy, K., and Othman, N. 2012. Aging and rattan-rubber composites. *BioResources*, 7(1), 841-858.

Kalaitzidou, K., Fukushima, H. and Drzal, L. T. 2007. A new compounding method for exfoliated graphite-polypropylene nanocomposites with enhanced flexural properties and lower percolation threshold. *Compos. Sci. Technol*, 67, pp. 2045–2051.

Karamat, S., Sonuşen, S., Çelik, Ü., Uysallı, Y., Özgönül, E. and Oral, A. 2015. Synthesis of few layer single crystal graphene grains on platinum by chemical vapour deposition. *Progress in Natural Science: Materials International*.

Khanlari, S. and Kokabi, M. 2011. Thermal stability, aging properties and flame resistance of NR-based nanocomposites. *J. App. Polym. Sci*. 119, pp. 855-862.

Kim, F., Cote, L. and Huang, J. 2010. Graphene Oxide: Surface Activity and Two-Dimensional Assembly. *Advanced Materials*, 22(17), pp.1954—1958.

Kim, H. W., Miura, Y. and Macosko, C. W. 2010. Graphene/polyurethane nanocomposites for improved gas barrier and electrical conductivity. *Chem. Mater*. 22, pp. 3441- 3450.

Kim, S., Do, I. and Drzal, L. T. 2009. Thermal stability and dynamic mechanical behavior of exfoliated graphite nanoplatelets-LLDPE nanocomposites. *Polym. Compos*, 31, pp. 755–761.

Kohjiya, S. and Ikeda, Y. 2014. Chemistry, manufacture and applications of natural rubber. *Cambridge: Elsevier*, pp.119-122.

Kuilla, T., Srivastava, S. K. and Bhowmick, A. K. 2009. Rubber/LDH nanocomposites by solution blending. *J. Appl. Polym. Sci*, 111, pp. 635–641.

Lee, C., Wei, X., Kysar, J. W., Hone, J. 2008. Measurement of the elastic properties and intrinsic strength of monolayer graphene. *Science*, 321, pp. 385–388

Lee, J., Chae, H., Won, Y. J., Lee, K., Lee, C., Lee, H. H., Kim, I. and Lee, J. 2013. Graphene oxide nanoplatelets composite membrane with hydrophilic and antifouling properties for wastewater treatment. *Journal of Membrane Science*, 448 pp. 223—230.

Lee, W. D. and Im, S. S. 2007. Thermomechanical properties and crystallization behavior of layered double hydroxide/poly(ethylene terephthalate) nanocomposites prepared by in-situ polymerization. *J. Polym. Sci. Pt. B Polym. Phys*, 45, pp. 28–40.

Li, J. C., Zeng, X. Q., Ren, T. H., Heide, E. 2012. The preparation of graphene oxide and its derivatives and their application in bio-tribological systems. *Lubricants*, 2, pp 137-161.

Li, X., Wang, H., Robinson, J. T., Sanchez, H., Diankov, G., Dai, H. 2009. Simultaneous nitrogen doping and reduction of graphene oxide. *J Am Chem Soc*, 131 (43), pp. 15939-15994.

Liang, J., Huang, Y., Zhang, L., Wang, Y., Ma, Y. and Guo, T. 2009. Molecular-level dispersion of graphene into poly(vinyl alcohol) and effective reinforcement of their nanocomposites. *Adv. Funct. Mater*, 19, pp. 2297–2302.

Lu, Y., Yang, X. and Su, B. 2013.Self-assembly to monolayer graphene film with high electrical conductivity. *Journal of Energy Chemistry*, 22 (1), pp. 52—57.

Malas, A., Das, C., Das, A. and Heinrich, G. 2012. Development of expanded graphite filled natural rubber vulcanizates in presence and absence of carbon black: Mechanical, thermal and morphological properties. *Materials & Design*, 39, pp.410-417.

Marcano, D. C., Kosynkin, D. V., Berlin, J. M., Sinitskii, A., Sun, Z., Slesarev, A., Alemany, L. B., Lu, W. and Tour, J. M. 2010. Improved synthesis of graphene oxide. *ACS nano*, 4 (8), pp. 4806—4814.

Novoselov, K. S., Falko, V. I., Colombo, L., Gellert, P. R., Schwab, M. G., Kim, K. 2012. A roadmap for graphene. *Nature*, 490, pp. 192–200

Novoselov, K. S., Geim, A. K., Morozov, S. V., Jiang, D., Zhang, Y., Dubonos, S. V. (2004). Electric field effect in atomically thin carbon films. *Science*, 306, pp. 666–669.

Olanipekun, O., Oyefusi, A., Neelgund, G. and Oki, A. 2014. Adsorption of lead over graphite oxide. *Spectrochimica Acta Part A: Molecular and Biomolecular Spectroscopy*, 118, pp.857-860.

Ooi, Z., Ismail, H. and Abu Bakar, A. 2014. Study on the ageing characteristics of oil palm ash reinforced natural rubber composites by introducing a liquid epoxidized natural rubber coating technique. *Polymer Testing*, 37, pp.156-162.

Ortiz-Serna, P., CarsÃ, M., Redondo-Foj, B. and Sanchis, M. 2014. Electrical conductivity of natural rubberâ€“cellulose II nanocomposites. *Journal of Non-Crystalline Solids*, 405, pp.180-187.

Palermo, V., 2013. Not a molecule, not a polymer, not a substrate… the many faces of graphene as a chemical platform. *ChemComm*, 49, pp.2848-2857.

Park, S., Dikin, D. A., Nguyen, S. T. and Ruoff, R. S. 2009.Graphene oxide sheets chemically cross-linked by polyallylamine. *The Journal of Physical Chemistry C*, 113 (36), pp. 15801—15804.

Pendolino, F., Armata, N., Masullo, T. and Cuttitta, A. 2015. Temperature influence on the synthesis of pristine graphene oxide and graphite oxide. *Materials Chemistry and Physics*.

Potts, J. R., Dreyer, D. R., Bielawski, C. W., Ruoff, R. S. 2011. Graphene- based polymer nanocomposites. *Polymer*, 52 (1), pp. 5-25.

Pramila Devi, D., Bipinbal, P., Jabin, T. and K.N. Kutty, S. 2013. Enhanced electrical conductivity of polypyrrole/polypyrrole coated short nylon fiber/natural rubber composites prepared by in situ polymerization in latex. *Materials & Design*, 43, pp.337-347.

Remesha, G.K., Sampath, S. 2009. Electrochemical reduction of oriented graphene oxide films: an in situ raman spectroelectrochemical study. *J Phys Chem C*, 113 (19), pp. 7985-7989.

Roberts, M. W., Clemons, C. B., Wilber, J. P., Young, G. W., Buldum, A. and Quinn, D. D. 2010. Continuum plate theory and atomistic modeling to find the flexural rigidity of a gaphene sheet interacting with a subsrate. *Journal of Nanotechnology*.

Rooj, S., Das, A., StÃ¶ckelhuber, K., Mukhopadhyay, N., Bhattacharyya, A., Jehnichen, D. and Heinrich, G. 2012. Pre-intercalation of long chain fatty acid in the interlayer space of layered silicates and preparation of montmorillonite/natural rubber nanocomposites. *Applied Clay Science*, 67-68, pp.50-56.

Sahoo, N. G., Cheng, H. K. F., Li, H., Chan, S. H., Judeh, Z. and Zhao, J. 2009. Specific functionalization of carbon nanotubes for advanced polymer nanocomposites. *Advanced Functional Materials*. 19(24): p. 3962-3971.

Schniepp, H.C., Li, J.L., McAllister, M.J., Sai, H., Herrera- Alonso, M., Adamson, D. H. 2006. Functionalized single graphene sheets derived from splitting graphite oxide. *J Phys Chem B*, 110 (17), pp. 8535–8539

Sheshmani, S. and Amini, R. 2013. Preparation and characterization of some graphene based nanocomposite materials. *Carbohydrate Polymer*, 96, pp. 384-359.

Shin, H. J., Kim, K. K., Benayad, A., Yoon, S. M., Park, H. K., Jung, I. S., Jin, M. H., Jeong, H. K., Kim, J. M., Choi, J. Y. and Lee, Y. H. 2009. Efficient reduction of graphite oxide by sodium borohydride and its effect on electrical conductance. *Adv Funct Mater*, 19, pp. 1987-1992.

Silwana, B., Horst, C., Iwuoha, E. and Somerset, V. (2015). Synthesis, characterisation and electrochemical evaluation of reduced graphene oxide modified antimony nanoparticles. *Thin Solid Films*, 592, pp.124-134.

Stankovich, S., Dikin, D. A., Dommett, G. H., Kohlhaas, K. A., Zimney, E. J., Stach, E. A. 2006. Graphene-based composite materials. *Nature*, 442, pp. 282–286.

Stankovich, S., Dikin, D. A., Piner, R. D., Kohlhaas, K. A., Kleinhammes, A., Jia, Y. 2007. Synthesis of graphene-based nanosheets via chemical reduction of exfoliated graphite oxide. *Carbon*, 45 (7), pp. 1558–1565.

Sun, L., Yu, H. and Fugetsu, B. 2012. Graphene oxide adsorption enhanced by in situ reduction with sodium hydrosulfite to remove acridine orange from aqueous solution. *Journal of Hazardous Materials*, 203-204, pp.101-110.

Tien, H., Luan, V., Lee, T., Kong, B., Chung, J., Kim, E. and Hur, S. (2012). Enhanced solvothermal reduction of graphene oxide in a mixed solution of sulfuric acid and organic solvent. *Chemical Engineering Journal*, 211-212, pp.97-103.

Titelman, G.I., Gelman, V., Bron, S., Khalfin, R.L., Cohen, Y. and Bianco-Peled,H., 2004. Characteristics and microstructure of aqueous colloidal dispersions of graphite oxide. *Carbon*, 43, pp. 641-649.

Tran, M., Yang, C., Yang, S., Kim, I. and Jeong, H. 2014. Influence of graphite size on the synthesis and reduction of graphite oxides. *Current Applied Physics*, 14, pp.S74-S79.

Tutorvista.com, 2015. Natural Rubber, Properties of Natural Rubber | Tutorvista.com. [online] Available at: http://www.tutorvista.com/content/chemistry/chemistry-ii/carbon-compounds/natural-rubber.php [Accessed 27 Mar. 2015].

Wang, H. and Hu, Y.H., 2011. Effect of Oxygen Content on Structures of Graphite Oxides, *Industrial & Engineering Chemistry Research*, 50(10), pp.6132-6137.

Wang, S., Tambraparni, M., Qiu, J., Tipton, J. and Dean, D. 2009. Thermal expansion of graphene composites. *Macromolecules*, 42, pp. 5251–5255.

Wang, X., Zhi, L., Mullen, K. 2008. Transparent, conductive graphene electrodes for dye-sensitized solar cells. *Nano Lett*, 8 (1), pp. 323–327.

Wanga, W. P. and Pana, C. Y. 2004. Preparation and characterization of polystyrene=graphite composite prepared by cationic grafting polymerization. *Polymer*, 45, pp. 3987–3995.

Wen, C., Zhao, N., Zhang, D., Wu, D., Zhang, Z. and Zhang, S. (2014). Efficient reduction and exfoliation of graphite oxide by sequential chemical reduction and microwave irradiation. *Synthetic Metals*, 194, pp.71-76.

Weng, W., Chen, G., and Wu, D. 2005. Transport properties of electrically conducting nylon 6/foliated graphite nanocomposites. *Polymer*, 46, pp. 6250–6257.

Williams, G., Seger, B., Kamat, P. V. 2008. TiO2-graphene nanocomposites. UV-assisted photocatalytic reduction of graphene oxide. *ACS Nano*, 2(7) pp. 1487–1491.

Wu, Z. S., Ren, W., Gao, L., Liu, B., Jiang, C., Cheng, H. M. 2009. Synthesis of high-quality graphene with a pre-determined number of layers. *Carbon*, 47 (2) (2009), pp. 493–499.

Xinmeng, A., Kezhi, L., Hejun, L., Jinhua, L., Qiangang, F., Yanhui, C., 2014. Graphene nanosheets synthesis via chemical reduction of graphene oxide using sodium acetate trihydrate solution. *Synthetic Metals*, 193, pp.132-138.

Xu, T., Jia, Z., Luo, Y., Jia, D. and Peng, Z. 2015. Interfacial interaction between the epoxidized natural rubber and silica in natural rubber/silica composites. *Applied Surface Science*, 328, pp.306-313.

Yu, A., Ramesh, P., Sun, X., Bekyarova, E., Itkis, M. E. and Haddon, R. C. 2008. Enhanced thermal conductivity in a hybrid graphite nanoplatelet-carbon nanotubes filler for epoxy composites. *Adv. Mater*, 20, pp. 4740–4744.

Zhang, H. B., Zheng, W. G., Yan, Q., Yang, Y., Wang, J. and Lu, Z. H. 2010. Electrically conductive polyethylene terephthalate/graphene nanocomposites prepared by melt compounding. *Polymer*, 51, pp. 1191–1196.

Zhang, K., Zhang, L. L., Zhao, X. S. and Wu, J. 2010. Graphene/polyaniline nanofiber composites as supercapacitor electrodes. *Chem. Mater*. 22, pp. 1392–1401.

Zhao, J., Liu, L. and Li, F. 2014. Graphene Oxide: Physics and Applications. *New York: Springer*, pp. 2-3.

Zhao, J., Pei, S., Ren, W., Gao, L., Cheng, H. M. 2010. Efficient preparation of large-area graphene oxide sheets for transparent conductive films. *ACS Nano*, 4 (9), pp. 5245–5252.

Zheng, W., Lu, X. and Wong, S. C. 2004. Electrical and mechanical properties of expanded graphite-reinforced high-density polyethylene. *J. Appl. Polym. Sci*, 91, pp. 2781–2788.

Zhou, M., Wang, Y., Zhai, Y., Zhai, J., Ren, W., Wang, F. 2009. Controlled synthesis of large-area and patterned electrochemically reduced graphene oxide films. *Chem Euro J*, 15 (25), pp. 6116–6120.

Zhu, Y., Murali, S., Cai, W., Li, X., Suk, J. W., Potts, J. R. and Ruoff, R. S. 2010. Graphene and graphene oxide: synthesis, properties, and applications. *Advanced materials*, 22 (35), pp. 3906-3924.

APPENDICES

Appendix A: Thermal Gravimetric Analysis of Nanocomposites

(a) TGA graph for NR

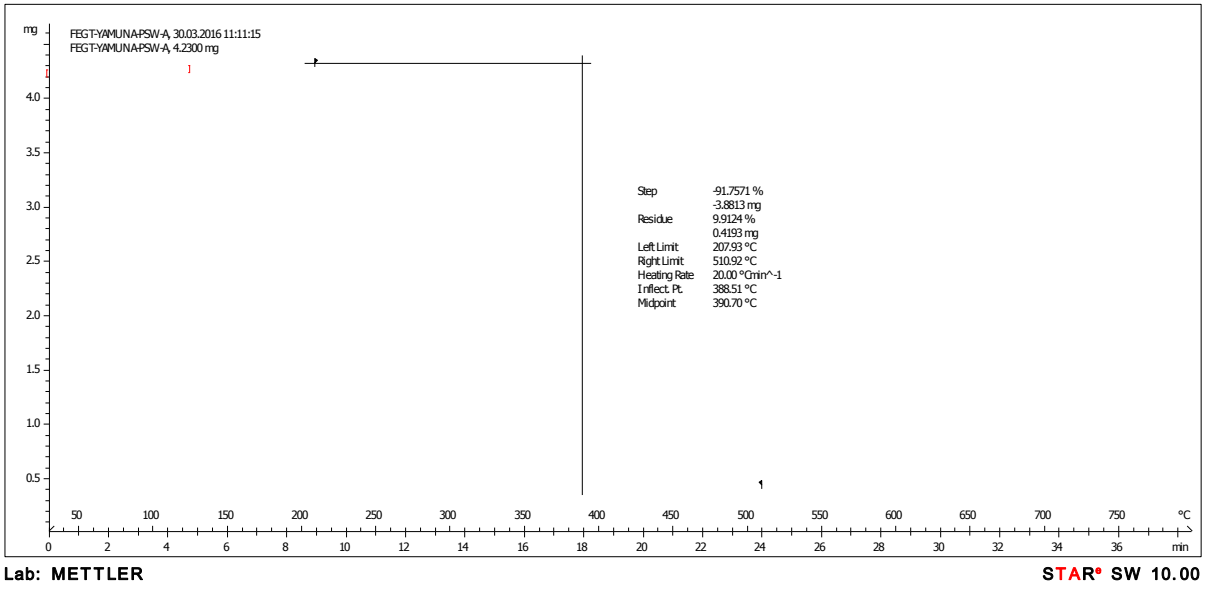

(b) TGA graph for NR/ 0.5phr rGO nanocomposites

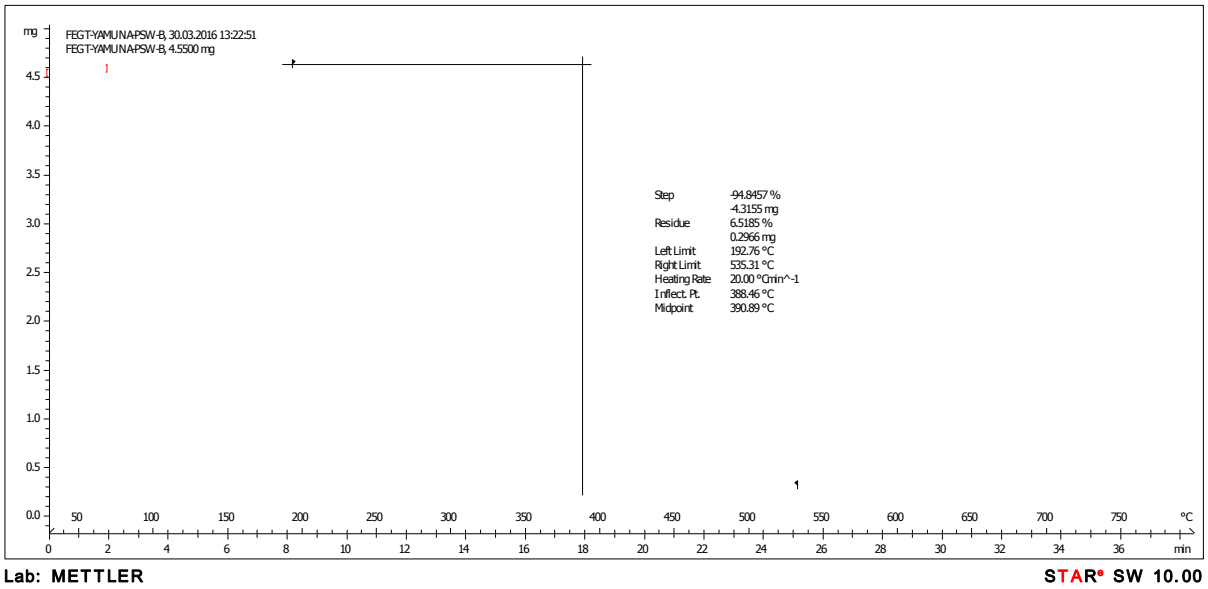

(c) TGA graph for NR/ 1.5phr rGO nanocomposites

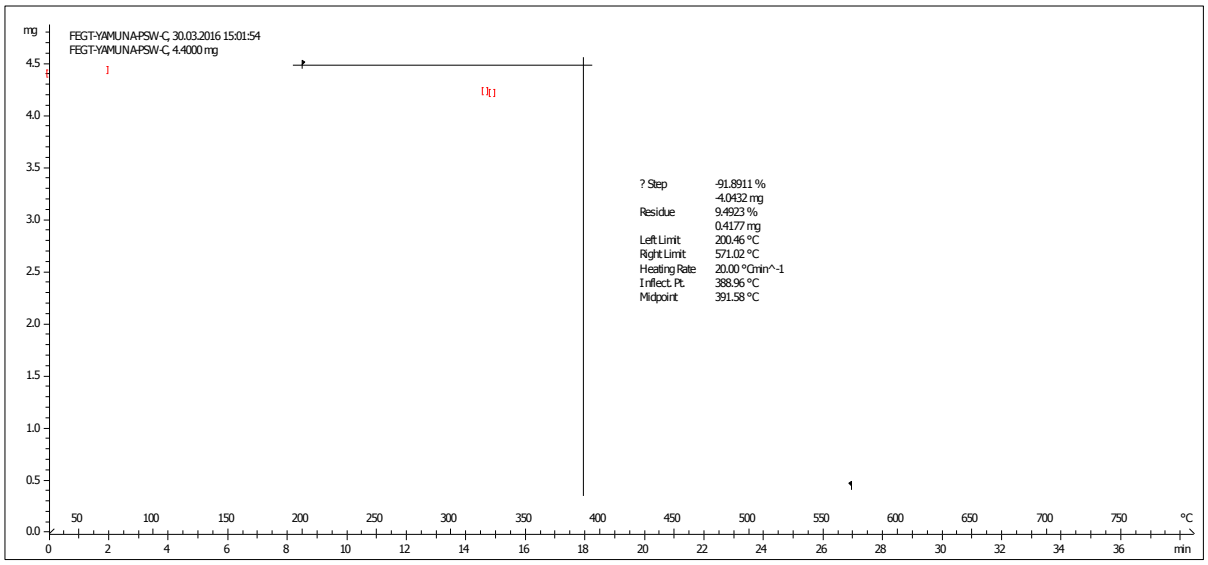

APPENDIX B: Rheometer Analysis of Nanocomposites

(a) Rheometer graph for NR

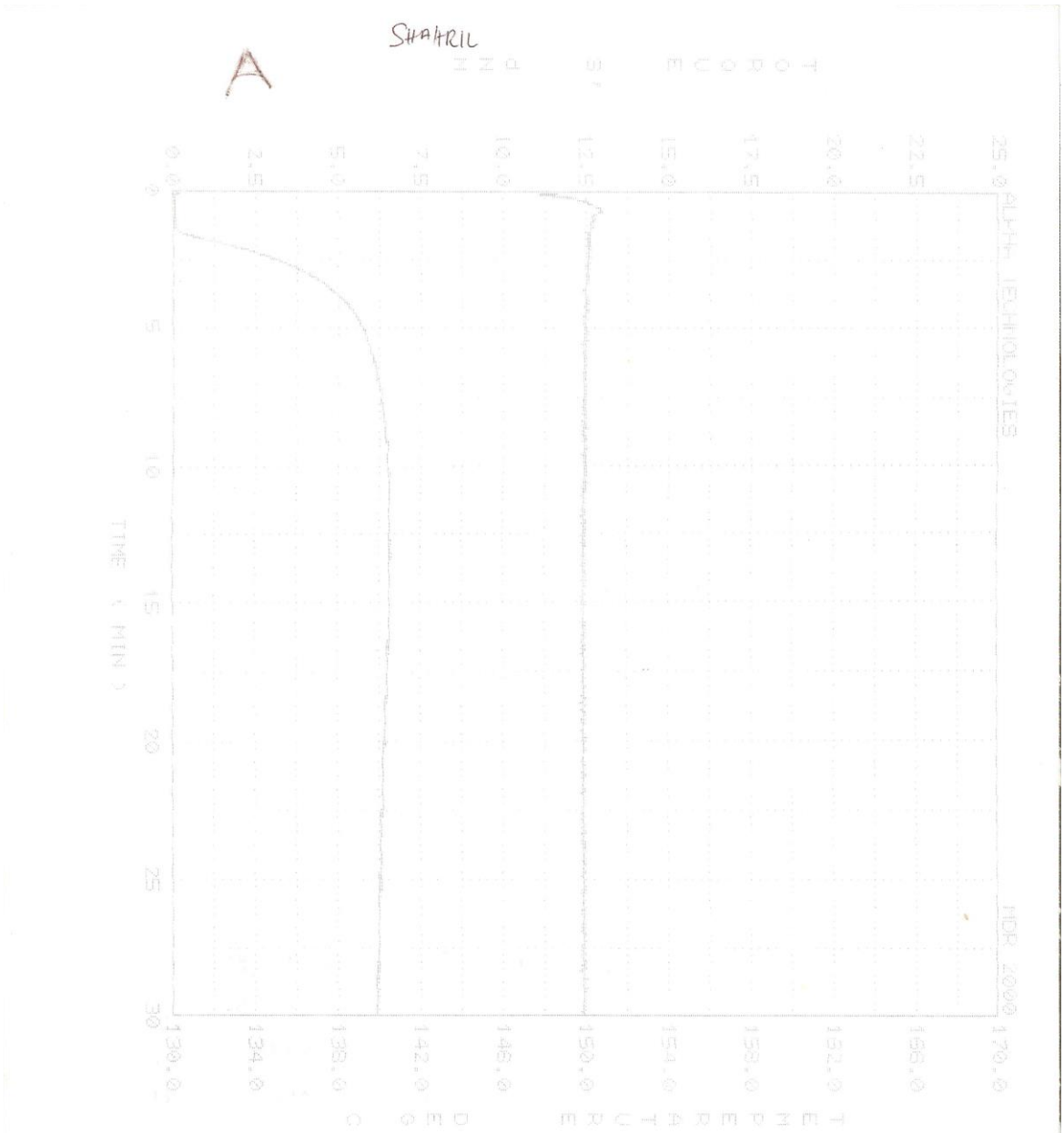

(b) Rheometer graph for NR/ 0.5phr rGO nanocomposites

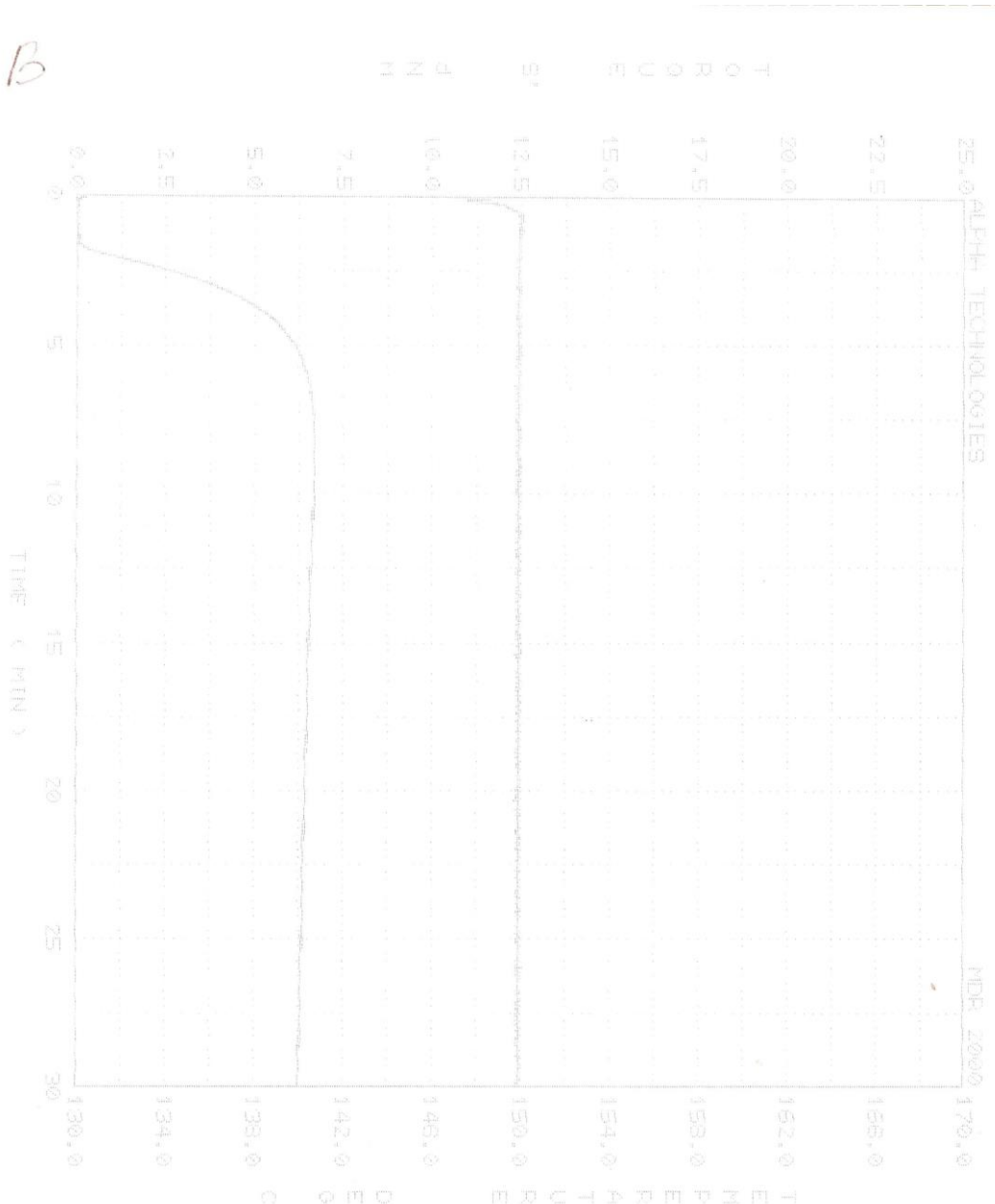

39AAA4398

° Temp:	150.0 C	ML:	0.05 dNm	S" @ML:	0.10 dNm	Tand @ML:	2.000
· Temp:	150.0 C	MH:	6.74 dNm	S" @MH:	0.04 dNm	Tand @MH:	0.006
tS1:	2.05 m.m	tS2:	2.34 m.m				
t10:	1.95 m.m	t50:	2.80 m.m	t90:	4.80 m.m		

(c) Rheometer graph for NR/ 1.5phr rGO nanocomposites

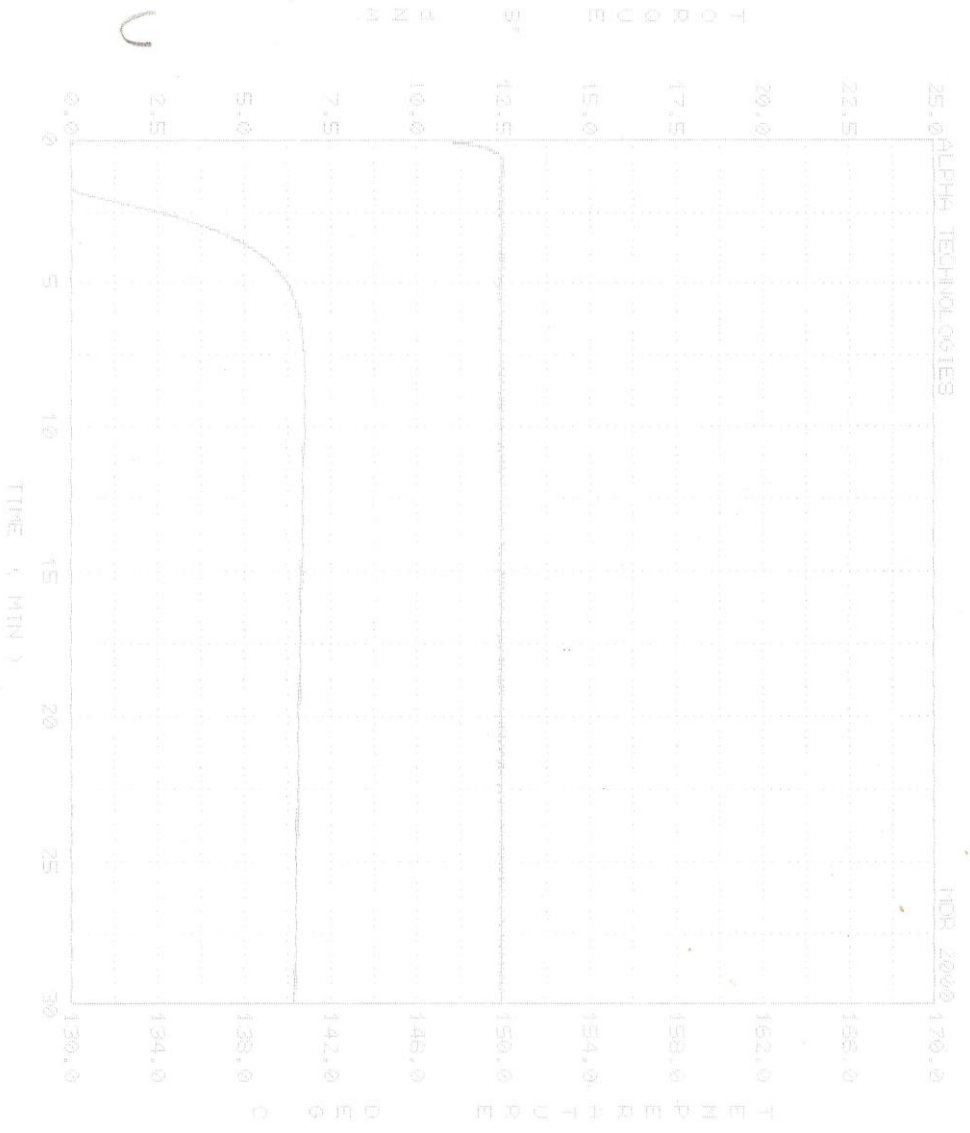

39AAA4398

° Temp:	150.0 C	ML: -	0.03 dNm	S" @ML:	0.07 dNm	Tand @ML:	-2.334
· Temp:	150.0 C	MH:	6.80 dNm	S" @MH:	0.06 dNm	Tand @MH:	0.009
tS1:	2.07 m.m	tS2:	2.34 m.m				
t10:	1.97 m.m	t50:	2.80 m.m	t90:	4.75 m.m		